MECHANISMS OF DISSEMINATION IN OVARIAN CANCER METASTASIS

Sara Al-Habyan

Faculty of Medicine

Division of Experimental Medicine

McGill University, Montréal

April, 2016

A thesis submitted to McGill University in partial fulfillment of the requirements of the Master's degree

ABSTRACT

Ovarian cancer (OvCa) persists as the most lethal gynecological cancer in women, with survival rates of 27% having undergone modest change in the past 30 years. During the progression of epithelial ovarian cancer (EOC), the most common type of OvCa, cells shed into the peritoneal cavity, which can later metastasize to distant organs. Disordered tumor blood vessels allow for lymphatic leakage into the abdomen, causing an accumulation of excess ascites supporting the growth of disseminated tumor cells (DTCs). DTCs are frequently found as multicellular spheroids that exhibit enhanced chemo-resistance and tumorigenicity over single cells. Little is known about how spheroids form, but single cell dissemination after epithelial-mesenchymal transition (EMT) and subsequent aggregation is a popular model. In this project, I undertook to understand how EOC cells detach and disseminate. Utilizing 2D and 3D cultures, I observed that cells were able to detach as either single cells or groups of cells. Moreover using ovarian orthotopic transplants and clonal analysis in mice, I confirmed polyclonal (multicellular) as a primary mode of detachment *in vivo*. I found few differences in the expression of epithelial and mesenchymal markers, indicating that overt EMT may not play a major role in detachment. However, SNAI1, was strikingly up-regulated, suggesting that it may function in a non-EMT capacity to support cell dissemination in absence of complete EMT. The results from this body of work provide a better understanding of the mechanisms of dissemination. Unravelling how cancer spheroids arise, survive and colonize will allow novel drug targeting, improving patient prognosis. I envision that this work can be used as a foundation for additional studies to improve patient outcome and response to chemotherapeutics.

RÉSUMÉ

Le cancer de l'ovaire (OvCa) demeure le cancer gynécologique le plus mortel avec un taux de survie de 27%, ce taux n'ayant pas changé depuis les 30 dernières années. Durant la progression du cancer épithélial de l'ovaire (EOC), le plus commun des OvCa, les cellules se dispersent dans la cavité péritonéale et peuvent par la suite causer des métastases à d'autres organes. Les vaisseaux sanguins tumoraux désordonnés occasionnent souvent une fuite du liquide lymphatique dans l'abdomen provoquant une accumulation d'ascites favorisant la croissance de cellules tumorales disséminées (DTCs). Les DTCs se retrouvent fréquemment sous forme de sphéroïdes multicellulaires présentant une chimiorésistance et une tumorigénicité accrues par rapport aux cellules individuelles. On en sait peu sur la façon dont les sphéroïdes se forment, mais le modèle selon lequel des cellules individuelles disséminées après leur transition épithélio-mésenchymateuse (EMT) s'agrègent subséquemment est le plus populaire. Dans ce projet, je cherchais à comprendre comment les cellules EOC se détachent et se propagent. À partir de cultures 2D et 3D, j'ai observé que les cellules se détachaient en cellules individuelles ou en groupes de cellules. De plus, en utilisant des greffes orthotopiques de tissu ovarien et l'analyse clonale chez la souris, j'ai démontré que le mode premier de détachement *in vivo* est polyclonal (multicellulaire). J'ai trouvé peu de différences dans l'expression des marqueurs épithéliaux et mésenchymateux, indiquant que l'EMT peut ne pas jouer un rôle majeur dans le détachement des cellules. Cependant, SNAI1 était remarquablement régulé à la hausse, ce qui suggère qu'il peut fonctionner dans une capacité non-EMT pour soutenir la propagation cellulaire en

l'absence d'EMT complète. Les résultats de ces travaux permettent de mieux comprendre les mécanismes de propagation. Élucider comment les sphéroïdes se forment, résistent et colonisent permettra le développement de médicaments ciblés. Je prévoie que ces travaux pourront être utilisés comme base pour des études additionnelles afin d’améliorer le pronostic des patients et la réponse aux traitements de chimiothérapie.

ACKNOWLEDGEMENTS

I would like to thank my supervisor Dr. Luke McCaffrey for accepting me as a student in his lab. His mentoring, support and patience were invaluable. He always inspired us to push our limits, network with diverse experts in science and pursue innovative ways to improve our research experience.

I also thank current and previous members in McCaffrey lab. Everyone is genuinely very kind hearted and fun to work with, the lab environment was contagiously refreshing and stimulating. Thank you to Carlis, Ruba, Maia, Sudipa, Li-Ting, Joseph, Andrew, Daya, and Christina for your support and help. I would also like to thank my TA lab mates for the long hours we spent in biology labs: Eni, Mina and Zahra for their support last year, in addition to our lab coordinator Anne-Marie Sdicu for her cheerful self and for translating my abstract to French. I would also like to extend my gratitude to Dr. Thomas Kucharski for his great patience in training me in my undergraduate project at Dr. Jose Teodoro's lab. I dedicate this work to my parents mama and baba, who selflessly sacrificed so much to help me get an excellent education. Thank you to my sister, my brothers, my munchkin nephews. Your presence helped me get through this journey.

My deepest thanks and gratitude go to my husband Nazem, my better half, for always believing in me, and for his unconditional love, encouragement and everlasting serenity. You are a beautiful blessing in my life.

CONTRIBUTIONS

OV90 and RH6 cells were obtained by the courtesy of Dr. Patricia Tonin.

Joseph Szymborski conducted and analyzed experiments done for OV90 and RH6 cells in figures (3.1.4, 3.2.1). Carlis Rejon and Dayananda Siddappa assisted in ovarian orthotopic surgeries. Christina Kalos assisted in analyzing data used to generate figures (3.1.1 B, 3.1.2 B).

Extended thanks to the Goodman Cancer Research Centre Histology core for providing training and equipment used in cryo-sectioning. I would also like to thank the Sorting facility in the Bellini Center and Ken McDonald, Diane Ethier and Camille Stegen for their assistance in cell sorting.

Dr. Peter Siegel provided the EMT biosensor vectors and 4T1 cells.

TABLE OF CONTENTS

LIST OF FIGURES

LIST OF ABBREVIATIONS

2D: 2-dimensional

3D: 3-dimensional

B2M: beta-2-microglobulin

BMP: bone morphogenesis protein

BRCA1: breast cancer 1

CAF: cancer-associated fibroblasts

CC3: cleaved caspase 3

CSC: cancer stem cells

CTC: circulating tumor cell

CTM: circulating tumor microemboli

DMEM: Dulbecco's modified eagle medium

DNA: deoxyribose nucleic acid

DTC: disseminated tumor cell

ECM: extra-cellular matrix

EGF: epidermal growth factor

EGF-R: epidermal growth factor receptor

EMT: epithelial-mesenchymal transition

EOC: epithelial ovarian carcinoma

ET-1: endothelin-1

FACS: fluorescence activated cell sorting

FBS: fetal bovine serum

FGF: fibroblast growth factor

FIGO: The International Federation of Gynecology and Obstetrics

GFP: green fluorescent protein

GSK-3β: Glycogen synthase kinase – 3 beta

HEPES: 2-[4-(2-hydroxyethyl)piperazin-1-yl]ethanesulfonic acid

HFG: hepatocyte growth factor

HGSC: high grade serous carcinoma

HS: heparan sulfate

IF: Immunoflourescence

MAPK: mitogen activated protein kinase

MET: mesenchymal-epithelial transition

MMP: matrix metalloproteinase

MSC: mesenchymal stem cells

OCT: optimal cutting temperature

OSE: ovarian surface epithelium

OvCa: ovarian cancer

P/S: penicillin streptomycin

Pak1: p21 activated kinase

PKD1: protein kinase D1

PBS: phosphate buffered saline

Poly-HEMA: Poly 2-hydroxyethyl methacrylate

RH6: radiation hybrid 6

ROCK: Rho associated protein kinase

ROCK-I: Rock kinase inhibitor

RNA: ribonucleic acid

RT: room temperature

RT-qPCR: reverse transcribed quantitative polymerase chain reaction

SEM: standard error of the mean

SDS-PAGE: sodium dodecyl sulfate polyacrylamide gel electrophoresis

STIC: serous tubal intraepithelial carcinoma

SWI/SNF: switch/sucrose non-fermentable

TBS-T: Tris buffered saline- tween20

TGF: transforming growth factor

VEGF: vascular endothelial growth factor

WHO: world health organization

YAP1: Yes associated protein 1

ZEB1: Zinc finger E-box-binding homeobox-1

GENERAL INTRODUCTION & LITERATURE REVIEW

1.1 OVARIAN CANCER: A BIOLOGICAL AND CLINICAL INTRODUCTION

1.1.1 OVARIAN BIOLOGY AND CANCER ORIGINS

Ovaries are reproductive organs in mammals that produce and release oocytes in a cyclic manner; a pair of ovaries connect to the body of the uterus by ovarian ligaments. The surface of the ovary is encased in a layer of epithelial cells, named the ovarian surface epithelium (OSE). During each ovulation cycle, the OSE ruptures to allow the release of the mature oocyte, followed by rapid healing and closure (Figure 1, Appendix 1). The oocyte transits through fimbria before passing by the fallopian tubes, finally landing in the uterus for fertilization [1]. The lining of the fallopian tubes and the OSE are both derived from a common embryonic origin in the pluripotent coelomic epithelium [2].

As proposed by the “incessant ovulation” theory, frequent ovulation and surface repair cycles contribute to the OSE’s susceptibility to malignant transformation [3, 4], which can give rise to epithelial ovarian carcinoma (EOC). Ovarian cancer continues to rank as the most lethal gynecological cancer in Canada amongst women, being the fifth most lethal of all cancer types in women combined. Due to its asymptomatic nature, tumor cells can survive, evolve and spread to multiple peritoneal, pelvic and, in rare occasions, to extra-abdominal organs before presenting any clinically detectable features [5].

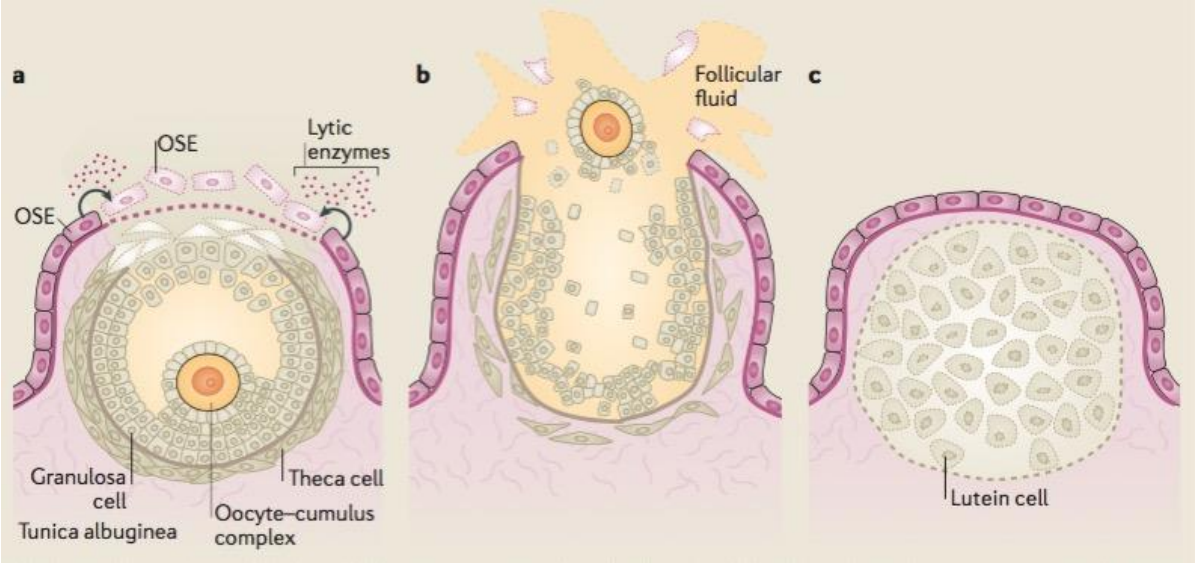

FIGURE 1: THE CYCLIC RUPTURE AND HEALING PROPERTIES OF THE OSE ALLOWS FOR OOCYTES TO BE RELEASED PERIODICALLY

A) The ovulatory phase: the OSE layer is triggered to begin dismantling through matrix degradation of the underlying basal lamina [6]. OSE cells are shed to allow for the release of the oocyte, due to the activity of lytic enzymes.

B) The rupture phase: The oocyte is released from the ovary through the ruptured epithelium into the peri-ovarian space [7].

C) The repair phase: wound closure and OSE re-construction through cellular migration and proliferation [8].

Repetitive rupture and repair trauma of the OSE are believed to promote cell proliferation, consequently harboring deleterious somatic mutations [9]. Consequently, the OSE undergoes invagination to form cortical inclusion cysts in the superficial ovarian cortex, exposing the cyst-lined OSE cells to activated stromal milieu [10] and OSE-secreted milieu [11], all which play a role in malignant transformation. However, a second model of ovarian carcinogenesis exists, where a combination of incremental mutational hits, namely involving Trp53, leads to malignant transformation of epithelial fallopian tube cells. This model is believed to account for most high grade serous carcinomas [12], and has been evaluated in *in vivo* mouse models [13, 14].

The international Federation of Gynecology and Obstetrics (FIGO) stage ovarian cancer as follows: Stage I includes ovary-confined disease, Stage II includes disease that has extended to the pelvis, Stage III encompasses microscopic involvement of abdominal surfaces and/or affected lymph nodes, and lastly Stage IV, where distant metastasis occurred and pleural effusions are cytologicaly positive [15].

EOC stands as the most common type of ovarian cancer, constituting 80% of ovarian cancer cases. The World Health Organization has categorized [16] EOC according to the predominant epithelial cell type. As the ovary epithelium undergoes metaplasia, it develops complex histology that resembles Müllerian duct-derived fallopian tube (serous EOC), endometrium (mucinous EOC), endocervix (endometrioid EOC), or vagina (clear cell EOC) [1]. Traditionally, it is believed that the OSE or cortical inclusion cysts are the only precursors to EOC. However, little evidence has proven the presence of OSE precursors to EOC, suggesting that carcinomas either arise de novo from

inclusion cysts [10], or are derived from extra-ovarian sources.

One hypothesis suggests that EOCs, namely high-grade serous carcinomas (HGSCs), could have fimbrial origins. Pre-neoplastic lesions termed serous tubal intraepithelial carcinomas (STICs) were identified in the fimbria of patients with normal ovarian histology, but were carriers of breast cancer 1 (BRCA1) and BRCA2 mutations [17-22]. The current model of fimbrial involvement in HGSC formation suggests that cortical inclusion cysts could arise form ectopic implantation of fimbrial STICs into the ovarian stroma, under the exposure of a milieu that promotes malignancy. On the other hand, the model supporting OSE invagination and entrapment might still apply, as some HGSCs were found to lack fimbrial STIC incorporation [18, 23].

1.1.2 MOLECULAR CLASSIFICATION OF EPITHELIAL OVARIAN CARCINOMA

Drs. Shih and Kurman [24, 25] have founded a model that categorizes EOC into two main types, which differ in the fundamental molecular pathways of carcinogenesis. **Type I cancers**, comprise low-grade serous, endometrioid, mucinous and clear cell tumors with low malignant potential. In contrast, **type II cancers** are poorly differentiated HGSCs. Type I cancers are usually associated with elevated survival times averaging around 82 months [26], indolent disease course, and increased resistance to chemotherapy. Interestingly, while type II cancers are initially chemo-sensitive to standard chemotherapy, patients have lower survival rates than Type I cancers, dropping from 82 to 30 months only [27].

Genetic changes in type I tumors seem to accumulate over time, fueling a conversion of benign epithelium into a malignant low-grade tumor [27]. Some mutations that type I

tumors frequently carry include BRAF, KRAS, ERBB2, and microsatellite instability [28]. Where active mitogen-activated protein kinase (MAPK) is expressed in the majority of low-grade tumors [29], it is expressed in only 41% of higher grade tumors. Moreover, p53 inactivations [25], BRCA 1/2 dysfunctions, amplification of the *AKT2* serine/threonine kinase and the phosphatidylinositol 3-kinase (*PIK3CA and PIK3R1*) genes [30] [31, 32] are amongst the most prevalent genetic alterations observed in high grade tumors.

1.1.3 CURRENT THERAPIES FOR OVARIAN CANCER

Patients presented with HGSC have a 5-year survival rate of only about 27% [33]. HGSC remains mainly incurable however as relapse occurs within 16– 22 months, with the gain of boosted chemo-resistance [33]. Standard therapy involves the use of chemotherapy agents, in addition to surgical intervention, to minimize the bulk of primary and secondary tumors, relieve the buildup of excess abdominal fluid (also known as ***ascites***), and prolong progression free survival.

There is an increasing trend to allow three or more cycles of chemotherapy to be administered before proceeding with surgery, largely to curb visceral damage, pain and other complications [33]. First-line combination chemotherapy regimen consists of carboplatin and paclitaxel, with promising new agents in clinical trials to be integrated. An example is a humanized monoclonal anti-body against vascular endothelial growth factor (VEGF), known as Bevacizumab [34]. VEGF has also been used as a measure of malignancy of cells in ascites [35], and recent findings suggest an improvement in the progression free survival of patients, but little evidence on its effect on overall survival

[36]. Despite all, a common fate dominates where the rebirth of numerous lesions invades abdominal organs, with large volumes of ascites becoming increasingly challenging to control. Nearly all patients become subjected to frequent *paracentesis;* drainage of excess abdominal fluid, with complications including continuous leakage from the drainage site and, occasionally, septic conditions following visceral damage [37].

1.2 ASCITES FORMATION AND MECHANISMS OF METASTASIS.

1.2.1 ORIGIN OF ASCITES

Derived from the Greek word *askites*, meaning bag-like, accumulation of fluid in the peritoneal cavity can arise from many pathologies, such as heart failure and tuberculosis, with a considerable minority (10%) associated with malignancy [33]. Causing symptoms such as early satiety and fullness, ascites buildup can be attributed to leaky vascular networks, lymphatic obstruction and associated stromal and immune cells [38]. Taken together, this creates a milieu for cancer cells that is supplemented with a dynamic reservoir of cytokines, chemokines, and extra-cellular matrix (ECM) fragments. In concert, this cocktail supports cell survival, growth, and maintenance of cancer cells before implantation at remote sites [39-42]. Malignant cells in ascites may adhere to the mesothelial layer lining the peritoneal cavity, which is mediated by CD44 [43, 44], β-integrins [45] and CA125 [46, 47] expressed on the ovarian cancer cell surface. While malignant ascites imposes substantial clinical challenges, its accessibility translates to a fertile source of tumor tissue during a course of patient treatment. Moreover, it can be exploited to identify prognostic and predictive biomarkers,

personalized medicine, and pharmacodynamic characteristics [33].

1.2.2 ASCITES COMPOSITION

Ascites fluid can be divided to two main constituents: a cellular fraction, and an acellular (soluble) fraction. The ascites cellular fraction offers a heterogeneous mixture of “resident” and “non-resident” cell populations, a phenomenon observed in other cancer microenvironments [37]. Tumor cells and cancer-associated fibroblasts (CAFs) fall in the resident cell category. Cells recruited from outside the tumor microenvironment however, including infiltrating immune cells and bone marrow-derived mesenchymal stem cells (MSCs) [48], are non-resident cells. Both populations are in interaction with each other through the secretion of soluble factors such as cytokines, enriching the tumor microenvironment [12]. In contrast to fibroblasts extracted from normal tissue, CAFs facilitate EOC cellular migration and invasion [49]. Furthermore, ovarian cancer associated MSCs were shown to promote tumor growth compared to their normal counterparts [50]. Abnormal production of bone morphogenic protein 2 (BMP2) can moderate MSCs role in ovarian cancer, where addition of recombinant BMP2 favored production of cancer stem cells (CSCs) expressing $ALDH^{+}CD133^{+}$[50].

Each population of cells has a specialized role and is able to flourish and communicate with other populations through soluble factors found in ascites. For example, IL-8 increases ascites formation in animal models [51], and IL-6 was not only shown to enhance tumor growth, migration, and invasion [52-54] but also to promote chemo-resistance [55, 56] and angiogenesis [57]. Clinically, high levels of IL-6 in ovarian cancer ascites was correlated with shorter progression-free survival [58-60], all

reflecting that the ascites microenvironment nurtures cancer cell growth.

1.2.3 THE METASTATIC CASCADE

Metastasis is the process through which cancer cells leave the primary tumor and seed in secondary sites, where cells compete with the host tissue to survive and proliferate. The most common metastatic sites in ovarian cancer are the peritoneal mesothelium, and visceral tissues including the liver and omentum, a large fatty sheet that drapes over the lower abdomen and pelvis [61]. High mortality rates in ovarian cancer are correlated with metastasis [62], and a mechanistic understanding of this process requires further investigation.

Classically in epithelial cancers, cancer cells acquiring invasive and migratory properties break through the basement membrane, through a process known as dissemination, upon successful departure from the primary site. Cells later enter the circulatory system (termed intravasation), where they are subjected to sheer forces, the innate immune system and oxidative stress. Cells at this stage are named circulating tumor cells (CTCs), or circulating tumor microemboli (CTM) when found in clusters. Surviving CTCs become mechanically entrapped in capillaries, before they breach the vascular wall and move into surrounding tissue (known as extravasation), or alternatively remain locally arrested [63]. Indeed, the complex process of metastasis requires a multitude of genetic changes and selective pressure for favorable traits through successive bottlenecks [64, 65]. EOC metastasis however stands unique from this cascade; as initial dissemination is not primarily haematogenous, rather is facilitated through exfoliation of primary tumor cells into the peritoneal fluid and accumulating ascites. In addition, OSE cells need not

breach a basal lamina to depart from the primary tumor, proposing that the genetic makeup required to gain metastatic-competency is distinct from cells that face the pressure of escaping through a basal lamina. Disseminated cancer cells isolated from ascites have been found to survive either as single cells or free-floating multicellular aggregates, commonly known as ***spheroids*** [27, 66]. Traditionally, complete epithelial-to-mesenchymal transition (EMT) was thought to be one of the main driving forces in dissemination from the primary tumor [67, 68]. In the next section, an overview of EMT is reviewed, followed by a discussion of EMT involvement in ovarian cancer disseminated cells.

1.2.4 INTRODUCTION TO EPITHELIAL-MESENCHYMAL TRANSITION

Initially described as 'epithelial to mesenchymal transformation' [69], this trans differentiation process is now commonly termed epithelial–mesenchymal transition (EMT) to emphasize its transient nature. This plastic process is also reversible, in a process termed mesenchymal-to-epithelial transition (MET). EMT is used to describe a fundamental change in phenotype and function, where epithelial cells lose their cell-cell adhesions and transit into a mesenchymal, migratory phenotype. EMT is essential in a number of non-pathological and pathological processes, exemplified in gastrulation, wound healing, fibrosis and cancer [70-72]. The fact that cells can undergo EMT fully or partially, permanently or transiently, demonstrates the flexibility of the process upon a spectrum or phenotypes rather than binary states. Hallmarks include epithelial cells losing their junctions [73, 74] and apical–basal polarity, and cytoskeletal reorganization to acquire cell shapes conducive to elevated motility and invasiveness under the regulation of particular genetic pathways [70, 71].

INITIATING AND REGULATING EMT FACTORS

In ovarian cancer, transforming growth factor (TGF) β, epidermal growth factor (EFG), hepatocyte growth factor (HGF), BMP4 and endothelin-1 (ET-1) have been shown to trigger EMT through different pathways [75]. In addition, a number of 'master' transcription factors are known to be activated in early EMT where they orchestrate the repression of epithelial genes and activation of mesenchymal genes, with possibilities of doing both, cooperating or regulating each other [74]. Factors include:

A) **SNAIL transcription repressors*:*** SNAI1 (or SNAIL), SNAI2 (or SLUG) and SNAI3 (or Smuc) induce the EMT program by binding to E-box DNA sequences within their carboxy-terminal zinc-finger domains [74, 76], resulting in inhibition of epithelial genes. For example, SNAI1 is involved in suppressing E-cadherin amongst other genes [77-83]. TGFβ and WNT family proteins, can activate SNAIL1 expression [74], and in turn, SNAIL can directly activate ZEB factors, another regulator of EMT. SNAIL was also found to be involved in ovarian cancer [84], where it can promote tumor growth [85], invasiveness [86] and resistance to chemotherapy [87].

B) **ZEB transcription factors*.*** ZEB1 and ZEB2 can repress or activate target genes [74, 76], which includes the recruitment of a C-terminal-binding protein (CTBP) co-repressor; or the Switch/sucrose nonfermentable (SWI/SNF) protein BRG1 which remodels chromatin [88]. ZEB2 has been shown to be up-regulated in EOC effusion [84, 89].

C) **miRNA-mediated control of EMT*.*** Non-coding miRNAs can inhibit the translation of target mRNAs, having downstream effects on regulating EMT

[90] MiR-29b and miR-30a for example can repress SNAIL expression [91], whereas miR-200 family represses ZEB1/2 expression [92]. Marchini et al have found that miR-200 family was a potential predictor of patient survival and can be used as a biomarker in stage I EOC [93].

Cooperatively, these factors and others result in down-regulation of E-cadherin and cytokeratins, along with the up-regulation of vimentin and proteases such as matrix metalloproteinase (MMP2 and MMP9) [94] to name a few, increasing ECM degradation and invasion.

The argument whether EMT is required however for dissemination and metastasis remains unresolved, as it becomes a topic of debate [95] whether observing it *in vitro* following artificial induction can be translated to a clinical context. In addition, many studies investigate the characterization of EMT starting with mesenchymal cells, which, by definition, does not meet the requirement of cells being initially epithelial. Recent studies have found that EMT was not a rate limiting step for invasion and metastasis, but rather plays a role in increasing chemo-resistance and enhanced nucleoside transporters in pancreatic [96] and breast cancer [97]. In addition, it has been shown that cells undergoing EMT can acquire resistance to senescence and apoptosis [70].

1.2.5 EPITHELIAL-MESENCHYMAL PLASTICITY IN OVARIAN CANCER

In the healing process post-ovulation, OSE cells gain fibroblast-like characteristics through undergoing EMT [98]. The down-regulation of E-cadherin expression is most commonly used as a surrogate marker of EMT, frequently accompanied by gain of mesenchymal markers such as vimentin. Despite intensive research about the

occurrence of EMT during dissemination, research results can often look contradicting. On one hand, enhanced tumor invasiveness was correlated with loss of E-cadherin expression, supporting a contribution of EMT in malignant transformation [99-101]. In addition, ovarian cancer spheroids expressing mesenchymal gene programs were shown to have enhanced mesothelial clearance [102].

On the other hand, early malignant change in OSE inclusion cysts associates with positive E-cadherin. A number of primary and secondary EOC tissues were reported to express E-cadherin [103, 104], with some studies reporting elevated E-cadherin in the metastatic site relative to its primary tumor [48]. Lastly, disseminated tumor cells in ascites from chemo-resistant ovarian tumors were found to exhibit enhanced E-cadherin expression [105].

These results argue that complete transition to a purely mesenchymal state may not be required in EOC cellular dissemination, given its different route compared to other epithelial cancers. These findings may also be explained by intermittent expression of E-cadherin during the progression of ovarian carcinoma.

1.2.6 ASCITES SPHEROIDS PROPERTIES

Following paracentesis, the process of draining excess abdominal fluid through insertion of a wild-bore needle through the peritoneal wall [33], spheroids are often observed in ascites in addition to single cells. Spheroids can collectively survive in suspension, and exhibit mesothelial-clearance characteristics by collective invasion [106]. However, spheroids were also found to have the ability to attach to the peritoneum, recruiting

independent vasculature networks [66]. Several findings suggest that spheroids demonstrate increased metastatic competency compared to single cells. Firstly, spheroids mimic traits of CSCs [107], concluded from their reduced proliferation rate and/or quiescence [108, 109], in addition to their decreased sensitivity to chemotherapy attributed to having limited drug penetration [110]. Secondly, cellular aggregation can dramatically help floating spheroids escape anoikis, consequently boosting their survival in suspension [111]. Not surprisingly, EOC spheroids were found to establish tumors at a comparable rate to single cells upon intraperitoneal injection in mouse models [112], validating that spheroids may survive and colonize in ascites [113]. Lastly, spheroids may cultivate cancer-initiating cells [114], making them a significant clinical target to investigate. Previous studies have indeed been insightful in characterizing spheroids, but fail to illustrate how spheroids arise *in vivo*. Despite having theories speculating that spheroids result from cellular aggregation in suspension following single-cell dissemination [115], evidence is severely lacking in the field.

Considering that spheroids are in transit following dissemination and prior to implantation, some studies have explored the mechanisms that regulate cellular adhesions between individual cells in spheroids. They were found positive for E-cadherin and EpCAM, coupled with low/negative expression of vimentin compared to single-cell population [105, 116]. Beta-1 integrins were also found to contribute to maintaining the cohesion of spheroids [117].

1.3 PROJECT DESCRIPTION, RATIONALE AND HYPOTHESIS

Over 75% of ovarian cancers have already metastasized at the time of diagnosis [27].

Elucidating the mechanisms driving metastasis is urgently needed to derive novel strategies to target the metastatic cascade. In particular, focusing on the early steps of dissemination as a rate-limiting step is crucial to prevent establishment of distant tumors. Understanding the cellular dynamics and cell-cell interactions are invaluable to address cellular dissemination, with particular focus on investigating cellular spheroids. The elevated metastatic potential of spheroids makes them an important target for research, with curiosity rising to identify underlying growth properties and therapeutic agents that could be effective against them [118, 119].

In this project, I aim to identify the mode(s) of dissemination in ovarian cancer cells, as single or groups of cells. Identifying the molecular mechanisms that govern each mode is a critical step towards our understanding of the unique ovarian metastatic profile and advancing patient therapeutics.

I hypothesize that ***Single and Collective modes of dissemination can drive ovarian cancer metastasis***. To test my hypothesis, I have three aims to address:

AIM1: Establish a model to study ovarian cancer dissemination *in vitro* and *in vivo*

OV90 cells were used as the main cell line of study, derived from the cellular fraction of ascites from a chemo-naïve epithelial ovarian carcinoma patient. It has been well characterized by morphological, cytogenic, and genomic profiles [120], and shown likely to represent high-grade serous ovarian carcinoma [121].

AIM2: Identify the mode(s) of dissemination in epithelial ovarian cancer cells

Using models established from Aim1, dissemination events were studied *in vitro* and *in vivo*. Confocal live imaging and ovarian orthotopic xenografts and clonal analysis were used to determine how cells detach from primary tumors.

AIM3: Elucidate the mechanisms driving dissemination

I explored the possibility of EMT involvement in ovarian cancer dissemination, using RNA and protein based techniques, in addition to genetic manipulation and drug screens to identify alternate pathways.

EXPERIMENTAL DESIGN AND METHODOLOGY

2.1 DNA CONSTRUCTS

pMD2.G encoding for the envelope protein VSV-G and psPAX2 are the packaging plasmids used for lentiviral production. PWPI was the lentivector used for transduction of fluorescent proteins GFP (green fluorescent protein), RFP (red fluorescent protein), and mCherry histone H2B under the EF1α promoter. Constructs were previously made in Dr. McCaffrey's laboratory.

2.2 CELL CULTURE

2.2.1 CELL LINES

All cell lines below were grown in humidified chambers at 37°C and 5% CO2. Growth media was changed every 2-3 days.

HEK293

Cell lines was obtained from ATCC. DMEM media was used for culturing, supplemented with 10% Fetal bovine serum (FBS) (Wisent), and penicillin/streptomycin (P/S, 100 U/mL) (Sigma) antibiotics (100U/mL).

OV90 and RH6

Cells were obtained by the courtesy of Dr. Patricia Tonin. Cells were cultured in Ovarian Surface Epithelium (OSE) medium (Wisent), FBS, P/S, 10mM 4-(2-hydroxyethyl)-1-piperazineethanesulfonic acid (HEPES) buffer (Wisent) and 4mM of L-glutamine (Wisent). RH6 cells were supplemented with 4 mg/mL Hygromycin (Wisent).

NIH:OVCAR-3 [OVCAR3] (ATCC® HTB-161™)

Cells were obtained from ATCC. Cells were cultured in 1640 medium (Wisent), supplemented with 15% FBS, 100U/mL P/S, and 0.01mg/mL insulin (Sigma).

2.2.2 DTC CHARACTERIZATION: VIABILITY AND COUNT

Cells were seeded in 6 well-plates, and allowed to attach overnight. Twenty-four hours post seeding, cultures were gently washed with sterile PBS, then given fresh media. Forty-eight hours post seeding, the growth media containing detached cells was collected in a 15 mL tube. Attached cells were trypsinized and collected in a separate 15 mL tube. To assess the viability of DTCs, DTCs were washed with PBS then centrifuged at 1000 rpm for 3 minutes, followed by re-suspension in 20µM of Ethidium homodimer-1 dye (Life Technologies) diluted in PBS and incubated at room temperature for 30 minutes. Afterwards, Calcein AM dye (Life Technologies) was added to a final concentration of 50µM and incubated for an additional 30 minutes. Fluorscence was imaged using a ZEISS Axiozoom 16 microscope. Live cells (detected by Calcein) were visible with green fluorescence, whereas dead cells (detected by Ethidium Homodimer) were visible with red fluorescence. Concentrations were optimized to minimize dye toxicity and overlap in signals in our lab.

Total cell numbers of either attached and detached cells were counted using a hemacytometer, and Trypan blue exclusion dye and the percentage of cell detached cells per well was calculated by the following formula: [(total number of DTCs/total number of attached cells)*100].

2.2.3 SPHERE FORMING ASSAY

Polyhema-coated low-adhesion plates were made by coating polystyrene culture dishes (Nunc) with a solution of Poly-HEMA (Poly 2-hydroxyethyl methacrylate; Sigma) in 95% Ethanol to a final concentration of 20mg/mL. Plates were left to dry overnight at 37°C, and stored at room temperature prior to cell seeding.

Cell monolayers were trypsinized using 0.25% Trypsin/EDTA (Wisent) for 20 minutes, with gentle mixing every two minutes using a P1000 pipettman. Cells were regularly visualized under a microscope to monitor disaggregation of cells into single cells. Once single cells are obtained, cells were filtered using 40µm filters (Fisherbrand), and 500 cells were seeded in 60 mm dishes (Nunc) coated with polyhema. Growth media consisted of either OSE media (recipe in section 2.2.1), or OSE media supplemented with EFG (20ng/mL), fibroblast growth factor (FGF, 20ng/mL), and heparan sulfate (HS, 0.0004%). Alternatively, Mammocult media (Stem Cell technologies) was used.

Spheres were grown for 14 days, with gentle mixing using a P1000 pipettman once a day.

2.2.4 HANGING DROP CULTURES

Cell suspensions were created with a concentration of 1 x 10^6 cells/mL in complete growth media. 30µL aliquots pipetted on the inside of a 10cm polystyrene culture dish lid (Nunc). 5 mL of PBS was added to the dish to avoid drying of the droplets. Droplets are collected 24 hours later rinsed with PBS (volume ratio of PBS to droplets was 10:1). For imaging, 30-50µL of the final solution was plated on Polyhema coated 8-chamber coverglass chambers (LabTek), with 500µL of growth media.

2.2.5 INHIBITOR TREATMENT

Cells were seeded at 80% confluency in 60mm dishes (Nunc). Twenty-four hours later cells were gently rinsed with PBS, and fresh media containing each inhibitor or its vehicle control was added as follows: [GM6001 (Millipore, 15µM), Thymidine (Calbiochem, 50µM), Blebbistatin (Sigma, 20µM), Rho Kinase inhibitor (Y27632 Santa Cruz, 10µ□M)]. Media containing DTCs was collected 24 hours following inhibitor addition. DTCs were counted and characterized as described above in section 2.2.2.

2.2.6 LENTIVIRUS PRODUCTION

HEK293-LT cells of passage numbers between 5 and 20 were plated at a density of 8x10^6 cells per 15-cm culture dish (Nunc). Cells were transfected 24-hours post plating

using the calcium phosphate method with 50µg of the target lenti-vector, together with the packaging plasmids: 15µg of pMD2.G and 37.5µg of psPAX in a 2.5 ml volume for each 15 cm dish. The virus was concentrated using polyethylene glycol (PEG8000, company) and the resulting pellet was re-suspended in OSE medium. The concentrated virus was mixed with a cell suspension, which were seeded on a culture dish for 72 hours.

2.3 RNA EXTRACTION AND QUANTITATIVE PCR (RT-QPCR)

Detached tumor cells were harvested from a confluent 15cm dish 72 hours post seeding. Attached cell monolayers were detached using 0.25% Trypsin/EDTA (Wisent), then re-suspended in complete growth media. Cells were collected by centrifugation at 300g for 5 minutes. RNA was extracted from cell populations using RNAeasy kit (QIAGEN), following manufacturer's instructions. Reverse transcription was performed using QIAGEN RT^2 strand kit following manufacturer's instructions. Lastly, QIAGEN PCR profiler array for human EMT signaling were used in conjunction with QIAGEN SYBR Green and an Eppendorf Realplex2 S real time cycler to run the real time PCR.

2.4 ANIMAL WORK

2.4.1 GENERAL ANIMAL HUSBANDRY

Experiments were done in accordance with the animal care guidelines at the Animal Resource Centre of McGill University under ethical approval.

Athymic nude mice [Crl:NU (NCr)-*Foxn1*^{nu}] were purchased from Charles River and housed in the Goodman Cancer Research Centre animal facility.

2.4.2 ORTHOTOPIC OVARIAN INJECTIONS

This procedure was conducted under aseptic conditions, using sterilized surgical tools. Accel-TB was used to maintain working surfaces and operating hands clean. Mice were injected sub-cutaneously with Carprofen analgesic (5µl/g body weight) 30 minutes prior to the procedure, and anaesthetized using isoflurane, with a nose cone used to maintain anesthesia throughout the procedure. Eye ointment (Alcon) was used to prevent corneal dehydration. During induction, Oxygen flowmeter levels were 0.8-1.5 mL/min, and isoflurane level was 4-5%. Under maintenance, Oxygen levels were adjusted to 0.4-0.8 mL/min and isoflurane levels reduced to 2-3%. Respiration rate was monitored visually and verified to be regular, thoracic and abdominal. Proper oxygenation was verified by mucous membranes and paws remaining pink in color. Before operating, the depth of anesthesia was assessed by testing the pedal reflex by pinching the toe pads and the paws of the animal with a pair of forceps. Isoflurane levels were adjusted as needed to insure reflexes were absent prior to operation.

With mice lying ventrally on a heated pad, a 1-cm skin incision was made dorsally using the spleen as landmark after sterilizing the area with chlorhexidine A smaller incision

was then made in the peritoneum, taking care not to damage internal organs. Forceps were used to gently pull out the ovarian fat pad and place it on sterile gauze resting on the skin. A 30G1 needle on a Hamilton syringe was used to inject 10µL of the cell suspension (0.75 x 10^6 in Geltrex (Invitrogen)) into the ovary, after securing the fat pad in place using forceps. The needle was then withdrawn, and tweezers were used to aid the fat pad retract into the peritoneal cavity. The peritoneum was then sutured using Vicryl coated absorbable sutures (Ethicon), and skin was closed by pinching both skin ends together and applying a coat of VetBond glue (3M). Following injections on both ovaries, the nose cone supply was switched to pure Oxygen to accelerate recovery. Sutures were sterilized in 70% ethanol.

2.4.3 BLOOD COLLECTION

Mice were anaesthetized in a Bell jar using isoflurane gas in a clean chemical hood. When the pedal reflex was absent, mice were removed from the jar and placed lying dorsally. The nose of the animal was placed in a cone containing isoflurane-soaked gauze to ensure that the animal remained under anesthesia throughout the procedure. The thorax of the animal was held between the thumb and the index fingers with the sternum pointing upwards. A 1 ml, 25G5/8 needle (BD), with the bevel pointing to the top, was used to penetrate the diaphragm ventrally at the center of the thorax directly under the tip of the sternum, at a 45 degree angle and a depth of 5-10mm. The syringe was swiftly brought nearly parallel to the thorax, and inserted fully, staying in the middle

of the thorax. One hand was then used to stabilize the syringe at the needle joint, while the other was used to withdraw blood at a constant rate; with caution not to build up high negative pressure. The syringe was then withdrawn at the same angle, the needle tip removed, and the blood emptied into an ice-cold collection tube. The animal was then removed from the nose cone and cerebral dislocation was performed.

2.4.4 CTC ISOLATION

Collected blood was mixed with dH_2O at a 1:10 volume ratio. The tube was inverted 5-10 times, followed by addition of concentrated PBS solution to have a 1X balanced concentration. The solution was then centrifuged at 4°C at 1000rpm for 3 minutes. The cells were washed with PBS then fixed in 4% paraformaldehyde (PFA; Bio Basic) for 20minutes on ice. Cells were washed and stored in PBS at 4°C until being imaged.

2.4.5 ASCITES COLLECTION

Euthanized animals were laid dorsally and an incision through the skin overlying the abdomen was made, with caution not to tear the peritoneal lining. A 1-mL Leur-Lok™ Tip (BD) syringe was used with a 23G1needle (BD) to penetrate the peritoneum, and fluid was collected and transferred to an ice-cold collection tube.

2.4.6 ISOLATION OF DTCS FROM ASCITES

Ascites fluid was centrifuged at 800 rpm for 3 minutes in a 1.5 mL Eppendorf tube. Approximately half of the supernatant was then removed, and washed with 1x PBS 5-8

times until the supernatant between washes was colorless. Cells were fixed in 4% PFA for 20 minutes on ice, followed by PBS washing prior to imaging.

2.4.7 TISSUE COLLECTION AND PROCESSING

Primary metastatic secondary tumors were resected and submerged in ice cold PBS before fixing in 4% PFA for 24 hours at 4°C. A portion of tissues was embedded in Optimal cutting temperature compound (OCT; VWR), freezed and stored at -80°C. Remaining tissue was processed, embedded and sectioned in paraffin by the Histology Core Facility of the Goodman Cancer Centre.

2.6 PROTEIN ANALYSIS

2.6.1 PROTEIN EXTRACTION

Cell culture dishes were placed on ice and rinsed with ice cold PBS twice before harvesting using a plastic scraper. Cells were centrifuged at 1000rpm for 3 minutes, and lysed in radio iummo-precipitation assay (RIPA) buffer (1mM EDTA, 0.5mM EGTA, 150mM NaCl, 1% Triton X-100, 0.1% Sodium deoxycholate, 0.1% SDS, 10mM Tris-HCl, pH 8.0) containing a protease inhibitor cocktail (Roche) on ice for 30 minutes. Lysates were centrifuged at 13,000 rpm for 10 minutes at 4°C. The supernatant was transferred to a clean tube, and protein concentration was quantified using Bradford protein Assay (BioRad). 6X Lamellae buffer was added to samples, and the lysates were stored at

-30°C until use. Lysates were boiled at 95°C for 5 minutes before separating by gel electrophoresis.

2.6.2 WESTERN BLOTTING

Thirty micrograms of protein lysate was separated by sodium dodecyl sulfate polyacrylamide gel electrophoresis (SDS-PAGE) for 30 minutes at 80V, followed by 150V for 90 minutes. Proteins were transferred to a nitrocellulose membrane for 2 hours at 120V. Ponceau Red (0.1% Ponceau Red in 5% acetic acid) was used to confirm successful transfer of total proteins. Membranes were blocked in 5% non-fat dry milk (Carnation) in Tris-buffered saline containing Tween20 (TBS-T: 50mM Tris, 150mM NaCl, 0.05% Tween20) for one hour in room temperature. SNAI1, ZEB1, Vimentin and E-cadherin antibodies were used according to manufacturer's recommendations, and were obtained from Cell Signaling Technologies: EMT kit.

Membranes were blocked in 5% weight/volume milk solution for 1 hour at room temperature. Membranes were incubated with primary antibodies in 5% weight/volume milk solution or BSA (BioShop) 5% weight/volume overnight at 4°C. Membranes were later washed for three times in TBS-T for 15 minutes. Secondary antibodies conjugated to horse-radish peroxidase were used against primary antibodies at a 1:5000 concentration in milk for 1 hour at room temperature. Membranes were again washed in TBS-T thrice for 5 minutes, and visualized using enhanced chemiluminescence (ECL) detection system (BioRad), and exposed to auto radiographic film (Santa Cruz).

2.7 IMMUNO - FLUORESCENCE AND IMAGING

2.7.1 STAINING 2D CELL CULTURES

SNAI1 antibody were obtained from Santa Cruz Biotechnology. ZEB1 antibody was obtained from Bethyl Laboratories. SNAI1 and ZEB1 Antibodies were used at a dilution of 1:100 in 5% goat serum in PBS. E-cadherin antibody was obtained from BD transduction, and was used at a dilution of 1:500 in 5% goat serum in PBS. ZO-1 and Vimentin antibodies were obtained from Cell Signaling, and were used at a dilution of 1:250 in 5% goat serum in PBS. Alexafluor 645-Phalloidin (Invitrogen) was used at a dilution of 1:100 in 5% goat serum/PBS to stain filamentous actin .

Cells were plated on 12mm No. 1.5 coverslips (Fisherbrand). Growth media was aspirated and cells were washed with PBS after a minimum of 24 hours post-seeding. Cells were fixed in 4% PFA for 20 minutes at room temperature. PFA was later disposed as hazardous waste. Cells were washed with PBS 3x 5minutes. Cells were permeabilized in 0.1% Triton X-100/0.1% BSA in PBS for 20 minutes at room temperature. Cells were then blocked for 1 hour at room temperature using 10% donkey serum in PBS and stained using primary antibodies diluted in 5% goat serum in PBS overnight at 4°C. Following three 15 minute washes in PBS, secondary antibodies were incubated for 1 hour at room temperature, diluted in 5% goat serum in PBS. Coverslips were counterstained with 1µg/ml DAPI in PBS for 20 minutes and washed twice for 15 minutes with PBS. Coverslips were mounted with 10µl 0.5% N-propyl gallate in 90% glycerol with 1X phosphate buffer (pH8.0), on glass slides (Fisherbrand: Superfrost

slides). Excess mounting media was aspirated from the edges of the coverslip, and sealed with clear nail polish (Revlon) and stored at 4°C until imaged.

2.7.2 LIVE-IMAGING HANGING DROP CLUSTERS

Cells were imaged in 8-well chamber coverglass plates (LabTek) as detailed in section 2.2.4 using a ZEISS LSM700 confocal microscope and a 20X 0.8NA objective lens. Cells were imaged every 10 minutes for 15-22 hours in a humidified chamber with 5% CO2 and heated to 37°C.

2.7.3 CRYOSECTIONING AND TILE-IMAGING

OCT embedded tissue blocks were sectioned using CryoJane (Leica Biosystems), using Feather S35 blades at -20°C. Twenty micrometer slices were allowed to adhere to glass slides (Leica X-tra), followed by drying overnight at 4°C. Slides were later immersed in PBS for 10 minutes at room temperature to solubilize OCT. Afterwards, slides were counter stained 1µg/ml DAPI in PBS for 20 minutes and washed twice for 15 minutes in PBS. Cells were mounted as described in section 2.7.1.

2.8 MICROSCOPY AND IMAGE ANALYSIS

To visualize the fluorescence across the tissue, tiled images were created using ZEISS LSM700 confocal microscope with a 10X objective lens.

ZEN black was used to obtain images from ZEISS LSM700 confocal microscope. AxioVision software was used to obtain images from the ZEISS Axiozoom 16 microscope. Movies were analyzed using ZEN blue software. Images were contrast-enhanced using ImageJ software (National Institute of Health, NIH), with uniform parameters applied across comparative images. Adobe illustrator CS6 was used to create figure panels.

2.9 STATISTICS

Statistical analyses and tests were conducted using Microsoft Excel. Two-tailed T-tests were used to assess significance at a minimum alpha value of 0.05. Data obtained from qRT-PCR was analyzed using the QIAGEN online tool GeneGlobe Data Analysis Center: Sample to Insight (http://www.qiagen.com/ca/shop/genes-and-pathways/data-analysis-center-overview-page/).

RESULTS

3.1 ASCITES-DERIVED OVARIAN CANCER CELL MONOLAYERS DISPLAY EPITHELIAL CHARACTERISTICS

EOC, the most common type of epithelial ovarian cancer, exhibits epithelial characteristics in both primary and secondary sites [104, 122]. We have therefore selected cell lines which have an epithelial phenotype as a representative of EOC, where monitoring phenotypic conversions throughout metastasis was possible.

Both OV90 and NIHOVCAR3 cells are derived from human ovarian cancer ascites that were found to be likely representative of EOC [121], and are chemo-naïve. In addition, we have also obtained a radiation hybrid (RH6) cell line that was derived from OV90 cells, but retains wild type chromosome 3p. RH6 cells exhibit a mesenchymal phenotype and, in contrast to OV90 cells, are non-tumorigenic [123]. Previous studies have characterized ovarian cancer cell lines as epithelial or mesenchymal based on the expression of E-cadherin (also known as CDH1), cytokeratin, and Vimentin, and reported that both OV90 and NIHOVCAR3 are epithelial [124]. To validate their phenotype in culture, we used a combination of immunofluorescence and immunoblotting to detect protein levels of E-cadherin, ZO-1, and Vimentin. We also examined ZEB1 and SNAI1, transcription factors that have been previously shown to promote mesenchymal phenotypes [125]. Both ZEB1 and SNAI1 commonly localize in the nucleus while having active transcriptional activity to drive EMT. As we expected, OV90 and NIHOVCAR3 cells expressed membrane bound E-cadherin as well as membrane-bound ZO-1 (Figures 3.1.1 , 3.1.2). This demonstrates that they both express tight and adherens junctions, hallmarks of epithelial phenotypes. Furthermore,

Vimentin was not detected by either immunostaining or immunoblotting methods (Figures 3.1.1, 3.1.2, 3.1.4). Although ZEB1 expression levels detected by western blot were minimal in OV90 cells, analysis by immunofluorescence indicated that its presence was variable with respect to expression and subcellular localization (Figure 3.1.1 A), and 48% of OV90 cells expressed nuclear ZEB1, with the remaining cells expressing uniform levels of cytoplasmic ZEB1 (Figure 3.1.1 B). Furthermore, 72% of OVCAR3 cells expressed nuclear ZEB1, with the rest of cells expressing uniform levels of cytoplasmic ZEB1 (Figure 3.1.2 B).

In addition, ZEB1 localization was found to vary with cell density levels where it appears to be nuclear, indicating its activity as a transcription factor, in lower densities. In higher densities however, ZEB1 is mainly located in the cytoplasm (Figure 3.1.5).

On the other hand, SNAI1 expression was detected both by immunoblot analysis and was found to be localized uniformly in the cytoplasm in 92% of OV90 cells and 78% or OVCAR3 cells (Figures 3.1.1 B, 3.1.2 B, 3.1.4). In contrast, RH6 cells expressed Vimentin but no E-cadherin nor ZO-1, as well as nuclear ZEB1 (Figure 3.1.3 and 3.1.4). This demonstrates that OV90 and RH6 have epithelial and mesenchymal phenotypes, respectively. The observation that ZEB1 and SNAI1 are expressed in cells with an overall epithelial phenotype (i.e. cell-cell adhesion, no Vimentin) was unexpected, but were excluded from the nucleus in the majority of cells, indicating that it is transcriptionally inactive. Moreover, recent reports indicate non-EMT roles for ZEB1 and SNAI1 in tumor-initiating events and stem cell properties [126, 127]. ZEB1 immunoflourescence experiments were conducted with two independent antibodies,

which gave similar and reproducible results. RH6 cells were used a positive control for ZEB1 staining, whereas cells stained with only a secondary antibody showed no background (data not shown). Constructs designed to knock down ZEB1 and SNAI1 will be tested in the future as a negative control for antibody signal specificity.

FIGURE 3.1.1. OV90 MONOLAYERS EXHIBIT AN EPITHELIAL PHENOTYPE.

(A) Immunofluorescent images of OV90 monolayers stained for the indicated cell markers. ZEB1 is localized to the nucleus in some cells. E-cadherin and ZO-1 are restricted to the cytoplasmic membrane. Scale bar = 50μm

(B) Quantification of the percentage of cells with ZEB1 (N=840 cells) or SNAI1 (N=668 cells) enriched in the nuclear (N>C) or cytoplasmic (C>N) compartments, or equally distributed (N=C).

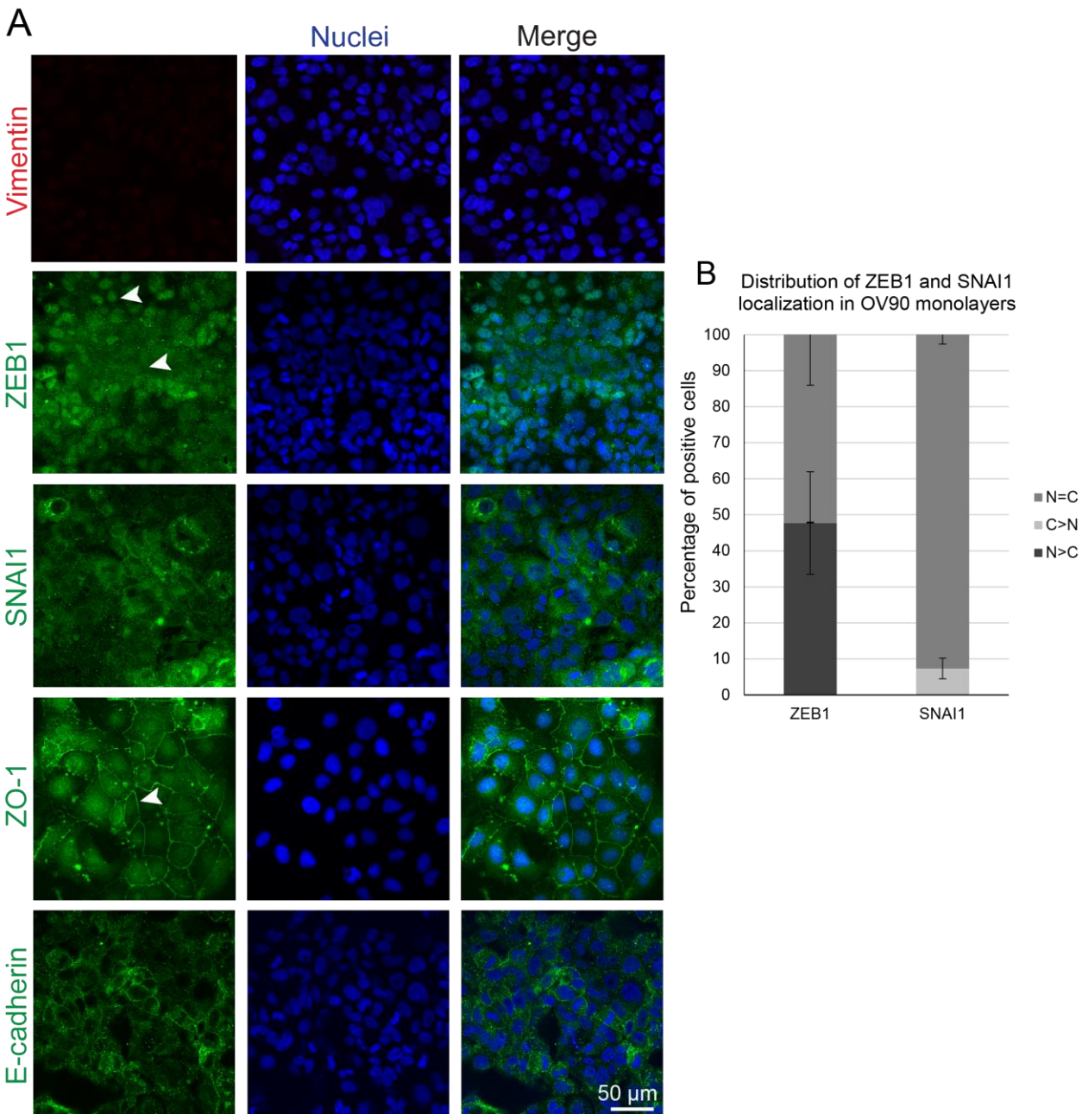
A
Nuclei
Merge
Vimentin
ZEB1
SNAI1
ZO-1
E-cadherin
50 µm
B
Distribution of ZEB1 and SNAI1 localization in OV90 monolayers
Percentage of positive cells
100
90
80
70
60
50
40
30
20
10
0
ZEB1
SNAI1
N=C
C>N
N>C

Figure 3.1.2. NIHOVCAR3 monolayers exhibit an epithelial phenotype.

(A) Immunofluorescent images of NIHOVCAR3 monolayers stained for the indicated cell markers. ZEB1 is localized to the nucleus in some cells. E-cadherin and ZO-1 are restricted to cell membranes. Scale bar= 100 μm.

(B) Quantification of the percentage of cells with ZEB1 (N=2064 cells) or SNAI1 (N=2208 cells) enriched in the nuclear compartment (N>C), cytoplasmic compartment (C>N), or equally distributed (N=C).

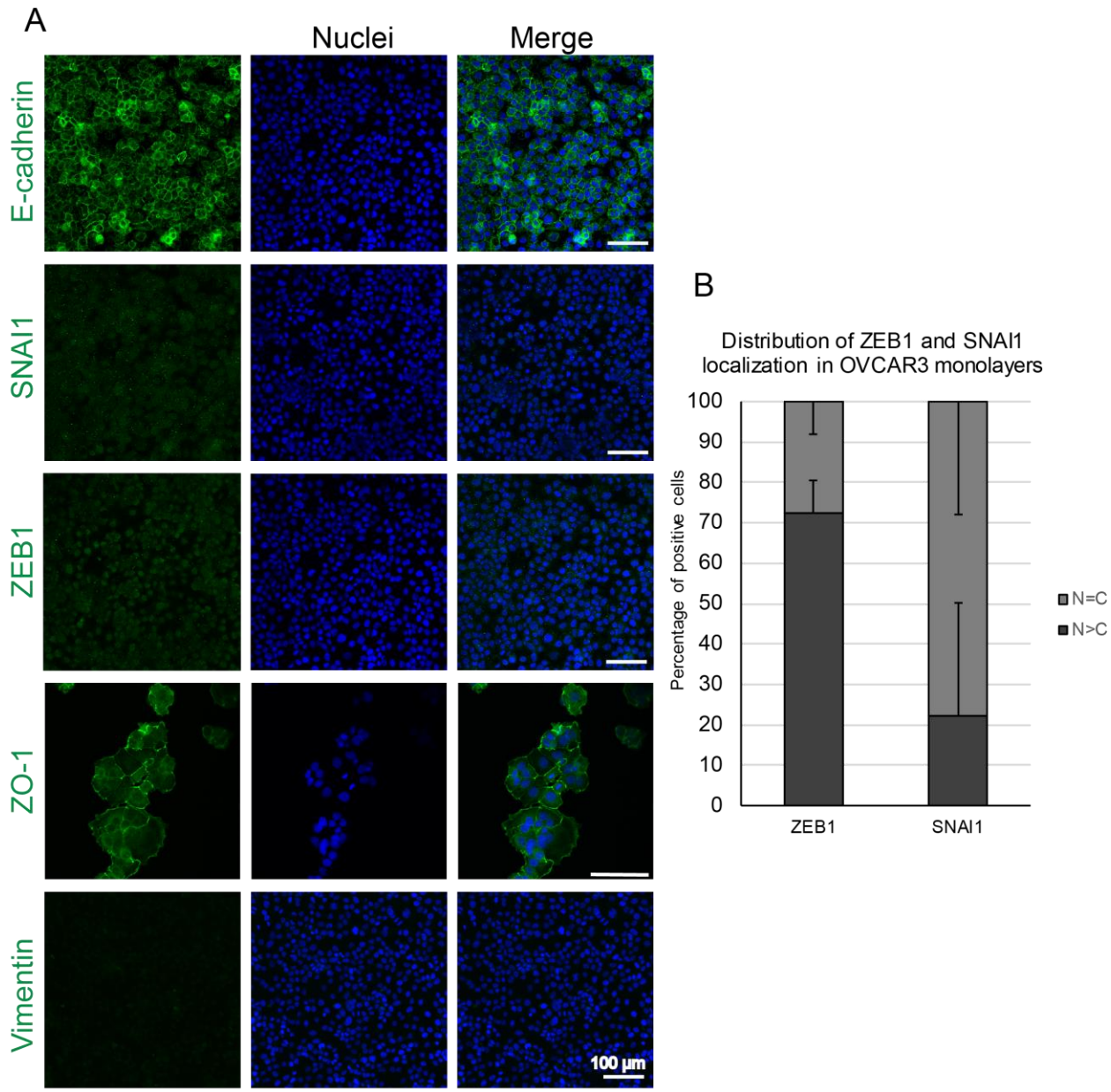
A
Nuclei
Merge
E-cadherin
SNAI1
ZEB1
ZO-1
Vimentin
100 µm
B
Distribution of ZEB1 and SNAI1 localization in OVCAR3 monolayers
Percentage of positive cells
100
90
80
70
60
50
40
30
20
10
0
ZEB1
SNAI1
N=C
N>C

Figure 3.1.3. A non-tumorigenic derivative of OV90, Radiation Hybrid 6 (RH6), exhibit a mesenchymal phenotype.

Immunofluorescent images of RH6 monolayers stained for the indicated cell markers. ZEB1 is localized to the nucleus. E-cadherin expression is absent, while ZO-1 immunostaining is diffused. Scale bar = 100 μm, unless otherwise noted.

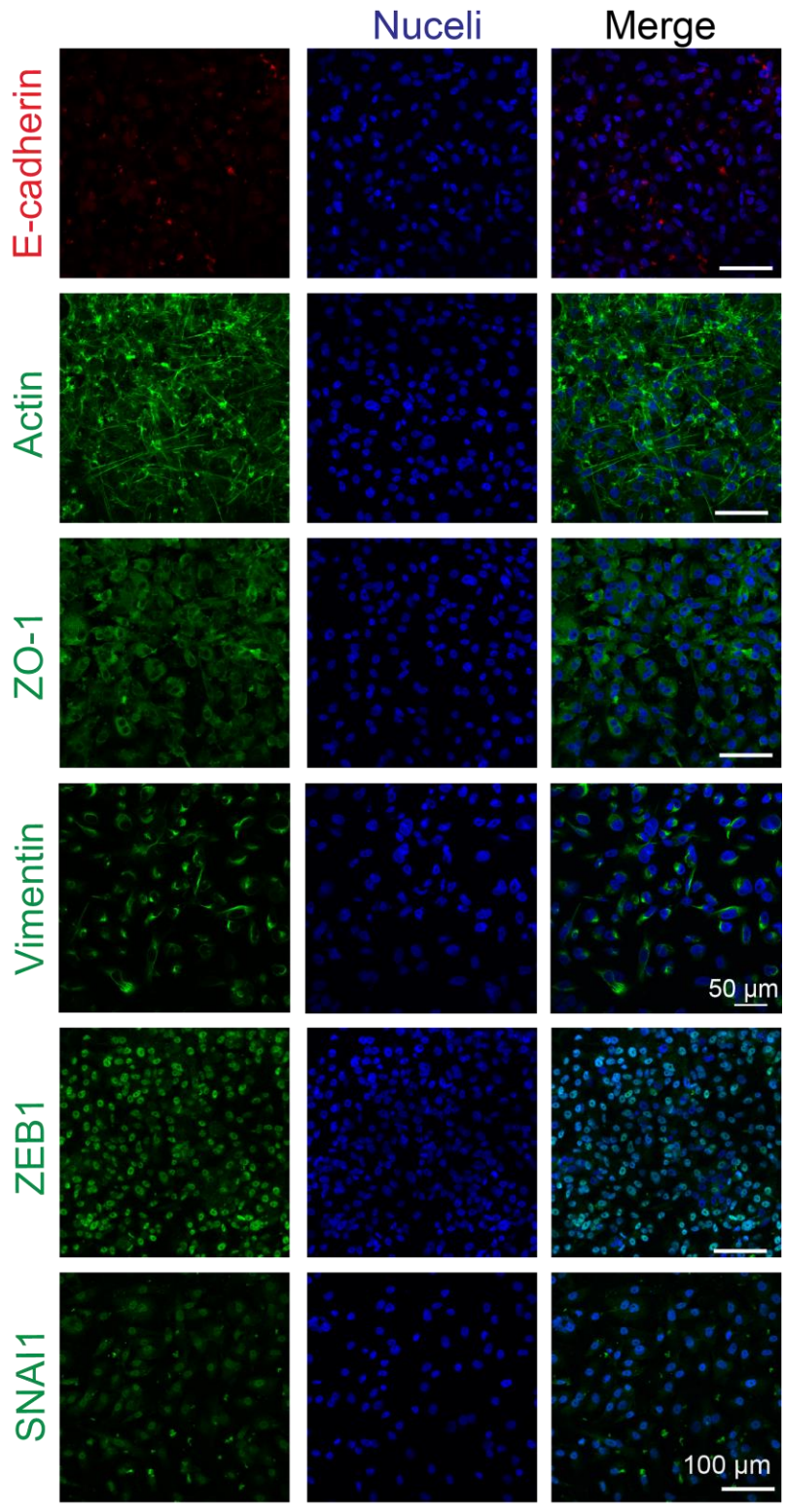
Nuceli
Merge
E-cadherin
Actin
ZO-1
Vimentin
ZEB1
SNAI1
50 µm
100 µm

FIGURE 3.1.4. DIFFERENTIAL EXPRESSION OF EPITHELIAL AND MESENCHYMAL MARKERS IN OV90 AND RH6 CELLS

Western blot of OV90 and RH6 cell lysates for the indicated cell markers.

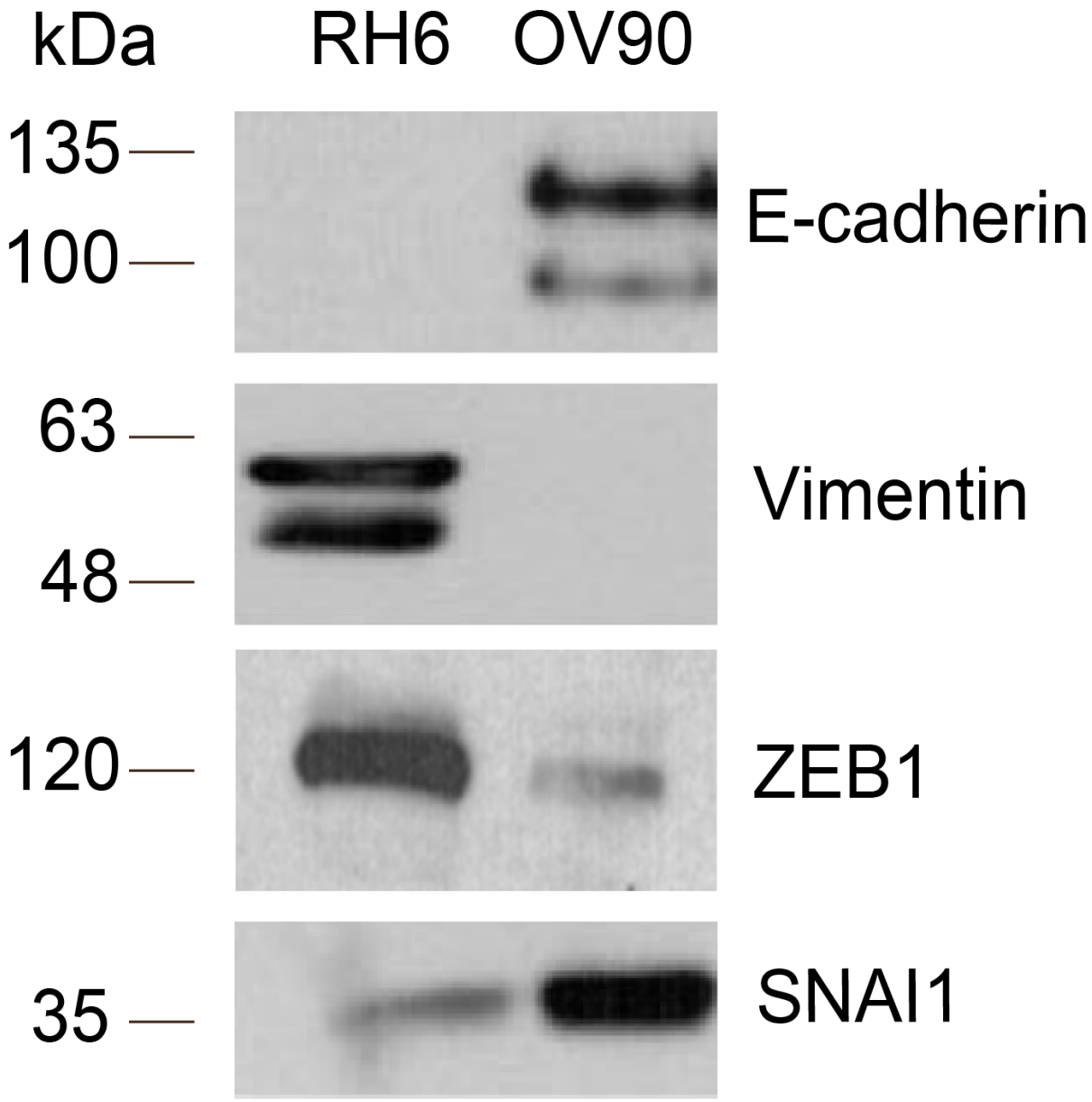
kDa
RH6
OV90
135
100
63
48
120
35
E-cadherin
Vimentin
ZEB1
SNAI1

FIGURE 3.1.5. ZEB1 SUBCELLULAR LOCALIZATION CO-VARIES WITH OV90 CELL DENSITY

(A) Immunofluorescent staining of ZEB1 in OV90 monolayers, localized either in the nucleus Field 1, or diffused in the cytoplasm Field 2. Different fields correspond to different magnifications and cell density levels. Scale bars = 50 μm.

(B) Quantification of OV90 cell density per area, graphed with the dominant ZEB1 localization per field (N=33 fields, $p<0.01$).

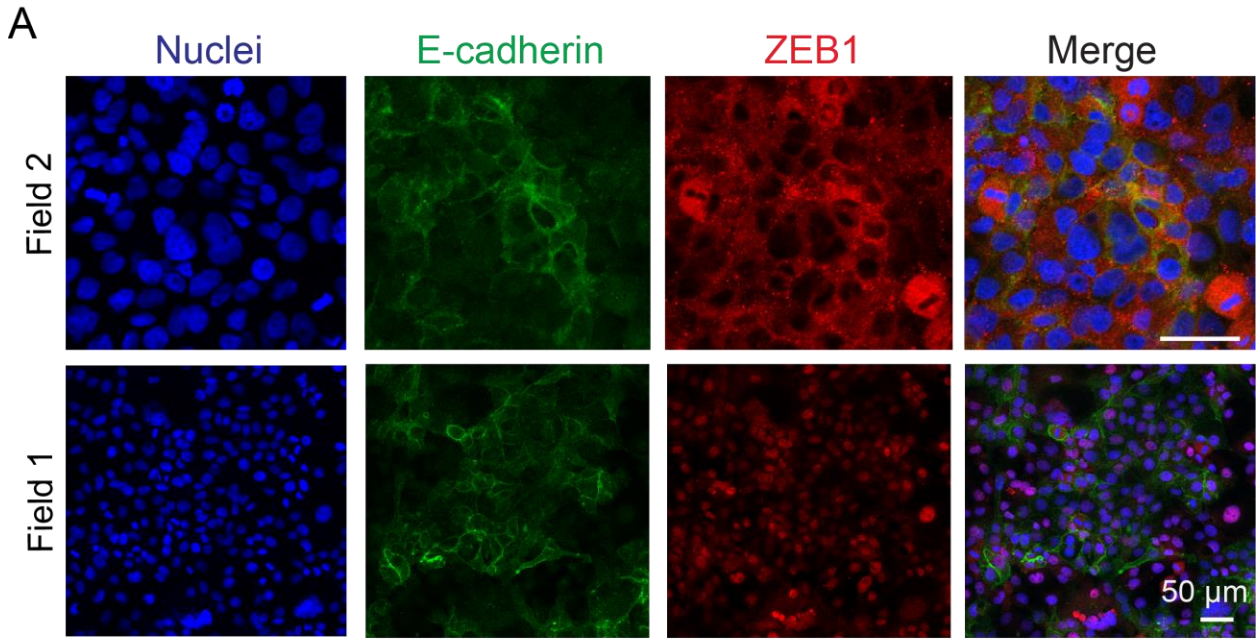
A
Nuclei
E-cadherin
ZEB1
Merge
Field 2
Field 1
50 µm

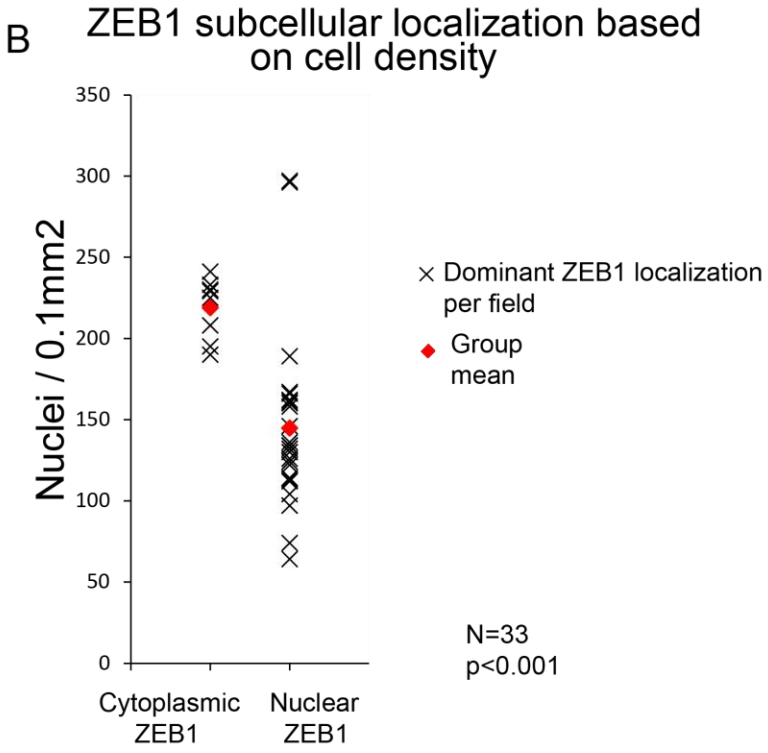
B
ZEB1 subcellular localization based on cell density
Nuclei / 0.1mm2
350
300
250
200
150
100
50
0
Cytoplasmic ZEB1
Nuclear ZEB1
Dominant ZEB1 localization per field
Group mean
N=33
p<0.001

3.2 OV90 AND NIHOVCAR3 CELLS ACTIVELY AND CONTINUOUSLY DISSEMINATE FROM CELLULAR MONOLAYERS *IN VITRO*

During characterization of these cell lines, I consistently observed cells floating in growth media above the cellular monolayers. This suggested that EOC may have the ability to spontaneously detach. I asked whether the floating cells could represent live cells that detached from the monolayer, or whether they were dead cells or debris. To determine this, I stained floating cells with Calcein AM and Ethidium homodimer fluorescent dyes. Calcein AM is cell permeable and is cleaved by cellular esterases to produce green fluorescence in live cells, whereas Ethidium homodimer is not cell permeable, but can enter perforated dead cells and label them with red fluorescence. Therefore, the presence and absence of each dye is a sensitive measure of cell viability (Figure 3.2.1A). The alive:dead ratio calculated was 3.4,2.4 and 2.2 for each of OV90, OVCAR3 and RH6, respectively (Figure 3.2.1B), indicating that these cells are largely alive in suspension. I refer to these cells as disseminated tumor cells (DTCs).

Mesenchymal cells exhibit reduced cell-cell adhesion and increased motility, which may make them more susceptible to detach and disseminate [125]. To determine if this was the case, I examined the frequency of DTCs in each cell line. DTCs were found to represent 5%, 2.5% and 3.1% of attached cells for each of OV90, OVCAR3 and RH6, respectively (Figure 3.2.1C). Interestingly, DTCs have been found in both single cells and multicellular clusters in suspension. This heterogeneity comes in close resemblance to tumor cells isolated from patient ascites, as both tumor spheroids and

single cell fractions have been recovered [105]. Molecular characterization of spontaneously generated DTCs in culture will be described in section 3.5.

FIGURE 3.2.1. EOC CELLS SPONTANEOUSLY SHED IN CULTURE.

(A) Detached cell viability test using Calcein AM (green/alive) and Ethidium Homodimer (red/dead) fluorescent dyes. Scale bar = 200μm. (B) Quantification of the ratio of alive/dead in disseminated cells. (C) Quantification of the percentage of dissemination in attached cells. N=3.

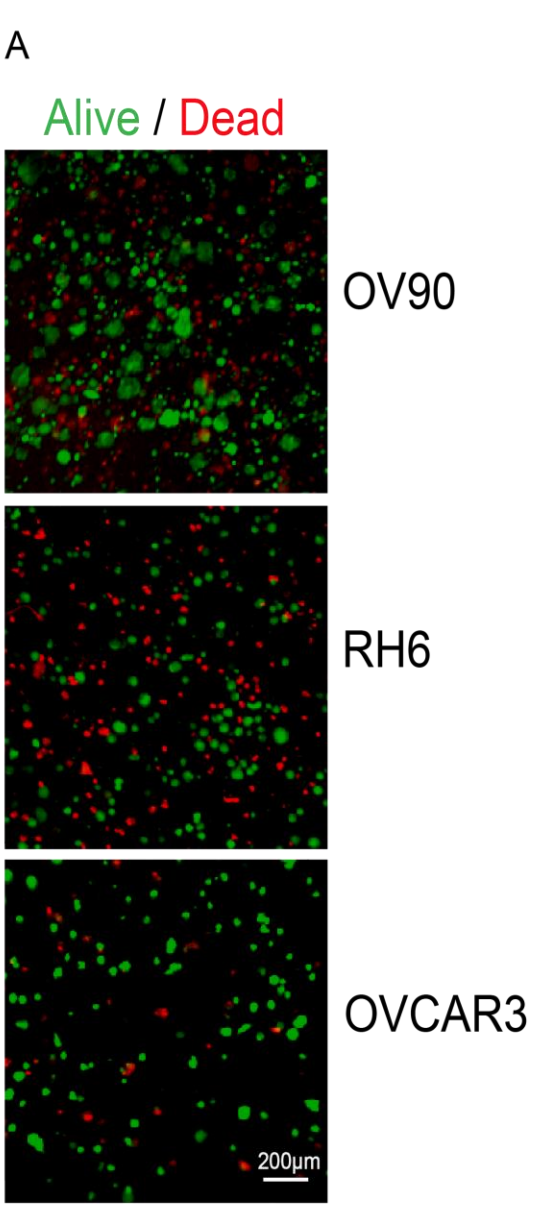
A
Alive / Dead
OV90
RH6
OVCAR3
200µm

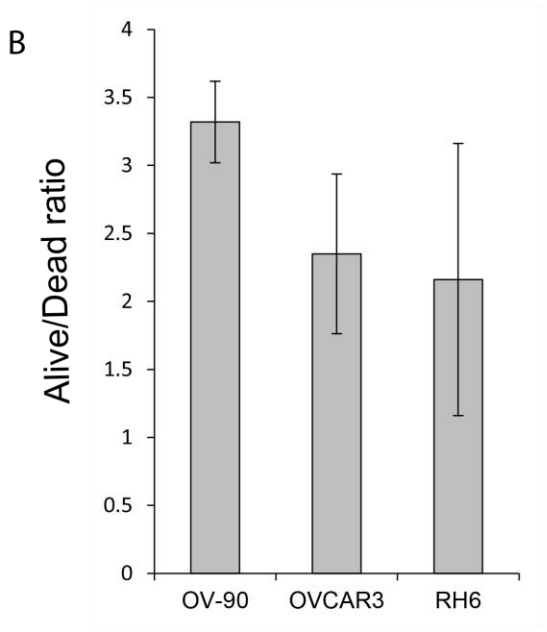
B
Alive/Dead ratio
4
3.5
3
2.5
2
1.5
1
0.5
0
OV-90
OVCAR3
RH6

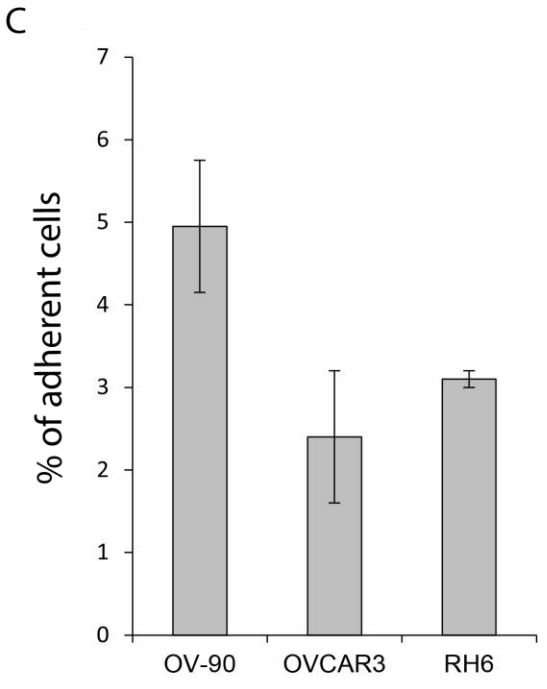
C
% of adherent cells
7
6
5
4
3
2
1
0
OV-90
OVCAR3
RH6

3.3 DIFFERENT MODES OF DISSEMINATION DRIVE OV90 METASTASIS *IN VITRO*

It has been established that cell clusters/spheroids isolated from patient ascites have increased metastatic potential compared to single cells, however the fundamental questions concerning their genesis has not been addressed yet. Two routes may lead to spheroid formation: 1) Cells may disseminate from the primary tumor as single cells, and proliferate in suspension where they may co-aggregate with other cells (single cell dissemination model). 2) Cells may *collectively disseminate*, where multiple cells detach from the primary tumor as a coherent unit, and survive as a spheroid in suspension (collective dissemination model). Indeed, understanding spheroid creation mechanisms may identify novel approaches to target metastatic stress and patient relapse.

We hypothesized that spheroids may arise from early points in the metastatic cascade, where *collective dissemination* may be occurring in addition to single cells dissemination. To determine how EOC cells detach, I performed live-imaging confocal microscopy. Cells were first modified to express GFP-tagged tubulin (GFP-Tub), and mCherry-tagged Histone H2B (mCherry-H2B). GFP-Tub facilitates visualization of microtubule-based mitotic spindles during cell divisions, while labelling of nuclei with mCherry-H2B enables efficient tracking of discrete cells. In culture, I noticed a number of cells that appeared rounded and loosely attached, and predicted that these may represent cells in the process of detaching. Visualization of GFP-Tub and mCherry-H2B indicated that these cells were mitotic (Figure 3.3.1). I therefore asked whether mitotic cells could contribute to detachment, either by reducing cell contact with the monolayer, or through mis-oriented cell divisions that results in one daughter cell dividing out of the

epithelial monolayer. However, shedding cells in this monolayer model were challenging to track in the Z-plane, since it was difficult to tell if cells were fully detached or tethered. Therefore, I decided to use 3D culture to track shedding of cells from tumorspheres. 3D tumorspheres have been routinely used to examine invasion in other solid cancers, like breast cancer [128], where spheres are traditionally embedded in ECM hydrogels. To generate tumorspheres, I utilized the hanging drop method, which has been adopted previously to mimic spheroids, and were found to have comparable tumorigenic ability compared to single cells *in vivo* [112]. However, I devised a new model to sustain spheres afterwards, where they were seeded in anchorage independent conditions. ECM hydrogels support basement membrane formation around spheres, which physiologically resembles a barrier that most solid epithelial tumors face. Given that EOC cells however are not limited by this barrier upon dissemination to ascites, I decided to seed tumorspheres on PolyHEMA coated plates to keep spheres in suspension. Not only was this model a closer physiological model to patient ascites, but it also provided greater resolution when imaged across multiple Z planes (stacks) to capture disseminating cells.

Approximately 39% of cells within tumorspheres were found to be actively proliferating, as denoted by positive nuclear Ki67 immunofluorescence staining. Furthermore, clusters generated by this method had minimal apoptosis, where 11% of cells stained positive for Cleaved Caspase 3 (CC3) (Figure 3.3.2). Imaging clusters over a period of 15-22hours, dissemination events were analyzed and categorized as single cell dissemination, or as collective dissemination when two or more cells leave the cluster, using labelled nuclei as a reference for counting cells. Of 38 events observed, 60% of

disseminating cells were in groups, whereas 40% of them were single (N=38, Fig 3.3.3: A, B, C). Moreover, none of the cells that detached did so after a mitotic event. Similarly, no mitotic cells detached, and all cell divisions were in the plane of the epithelium (Fig 3.3.1 D). Together, these findings support the use of hanging drop clusters as active physiological entities, and provide evidence for the presence of both single and collective cell dissemination modes *in vitro*.

FIGURE 3.3.1. OV90 MONOLAYERS EXHIBIT ACTIVE PROLIFERATION AND CYTOSKELETAL DYNAMICS.

Live-imaged OV90 monolayers over 24 hours. Cells were labelled with GFP-tubulin and mCherry histone. Cells undergoing mitosis, denoted by arrows, exhibit a rounded morphology.

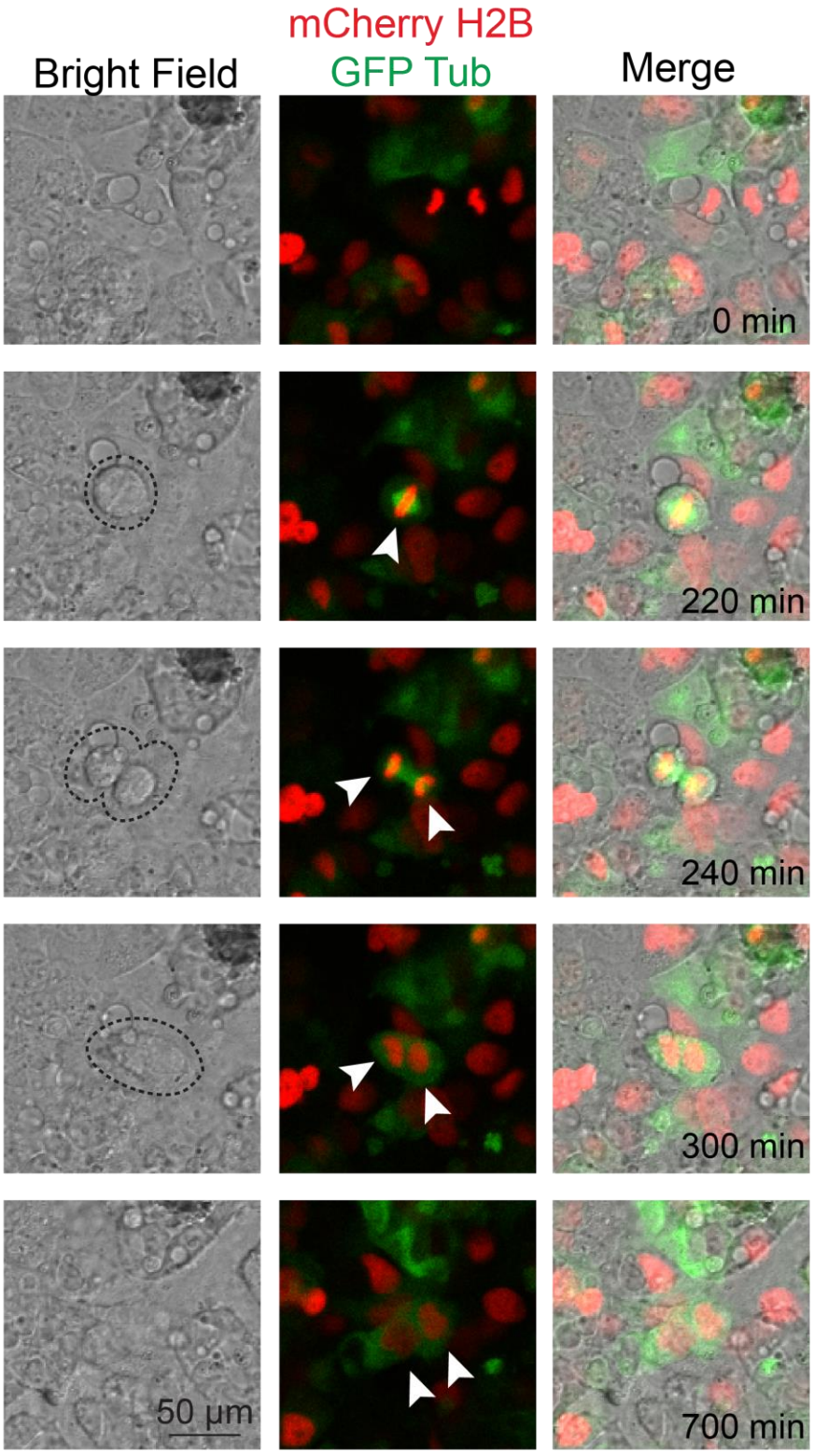
Bright Field
mCherry H2B
GFP Tub
Merge
0 min
220 min
240 min
300 min
700 min
50 µm

FIGURE 3.3.2. OV90 TUMORSPHERES ACTIVELY PROLIFERATE

(A) Immunofluorescent staining of tumorspheres for proliferation (Ki67) and apoptosis (cleaved Caspase 3 (CC3)) markers.

(B) Quantification of the number of cells expressing Ki67 and cleaved caspase 3 (CC3), a marker of apoptosis. N= 7. Scale bar = 50 μm.

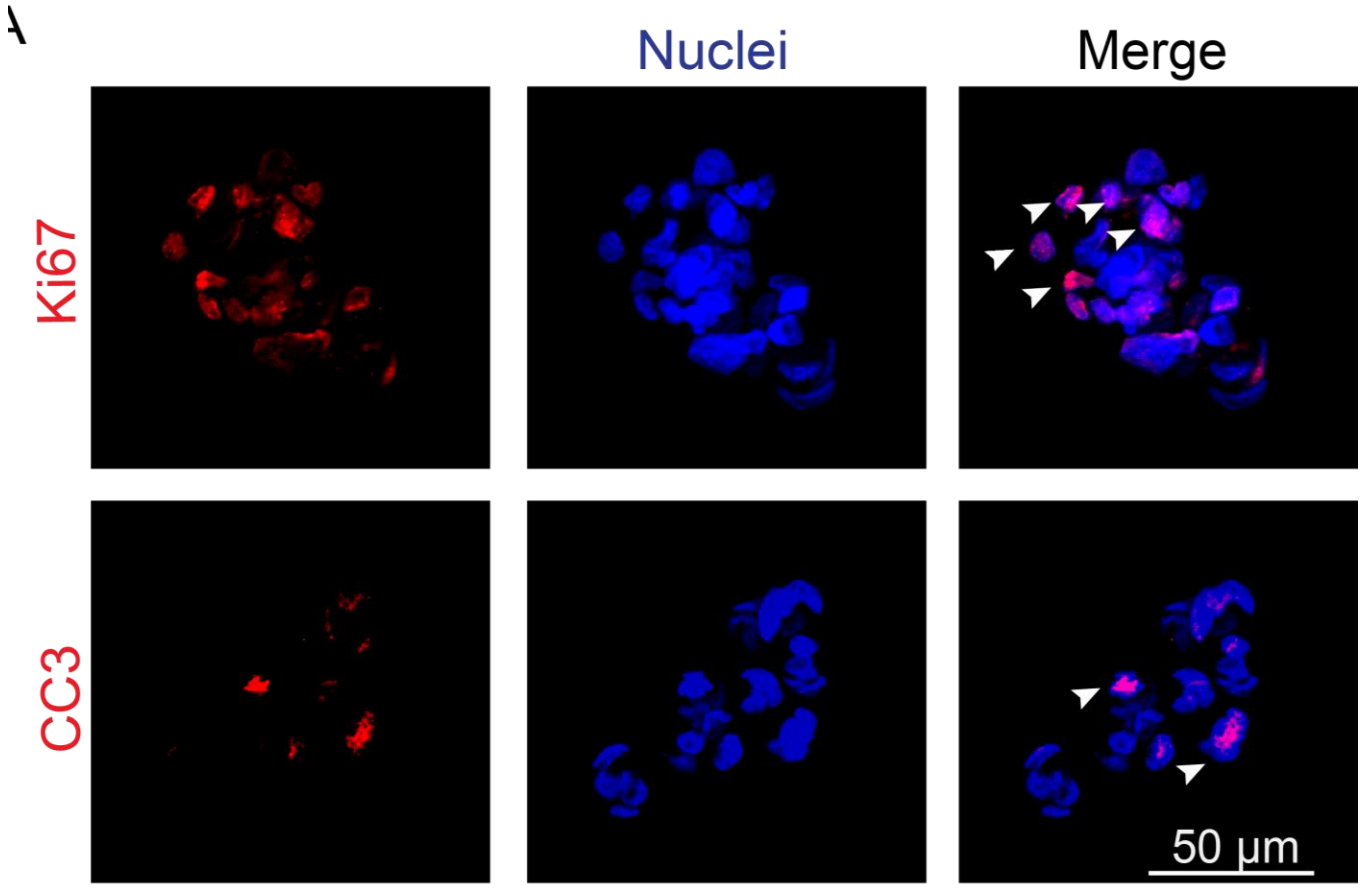
A
Nuclei
Merge
Ki67
CC3
50 µm

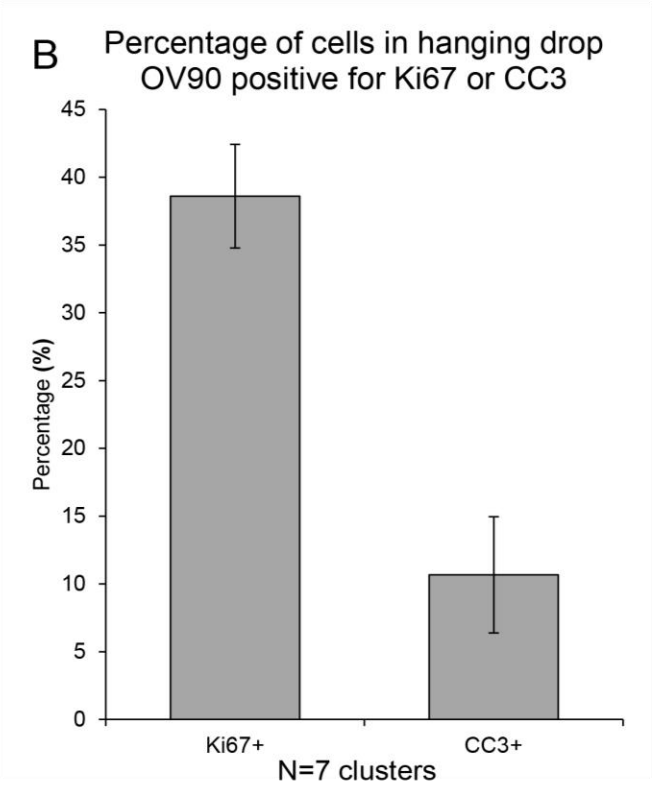
B
Percentage of cells in hanging drop
OV90 positive for Ki67 or CC3
Percentage (%)
45
40
35
30
25
20
15
10
5
0
Ki67+
CC3+
N=7 clusters
Error bars= SEM

FIGURE 3.3.3. SINGLE AND COLLECTIVE DISSEMINATION OF OV90 CELLS IN TUMORSPHERES.

Live-imaging of OV90 tumorspheres in low-adhesion conditions over 22 hours.

(A) Single cell dissemination.

(B) Collective cell dissemination.

(C) Quantification of fraction of dissemination events as single or collective.

(D) Mitotic cells at tumorspheres surfaces. Spindle orientation is parallel to tumorspheres surface (arrows). Scale Bars = 50μm.

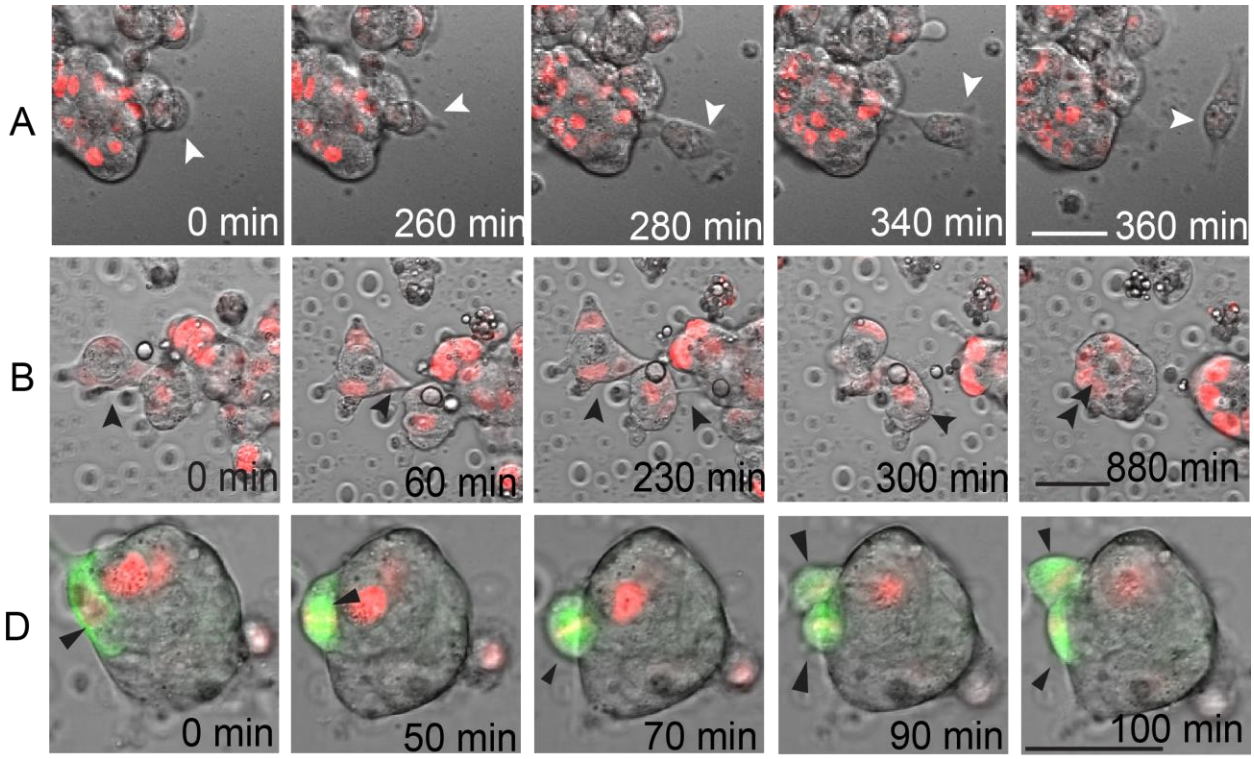
A
0 min
260 min
280 min
340 min
360 min
B
0 min
60 min
230 min
300 min
880 min
D
0 min
50 min
70 min
90 min
100 min

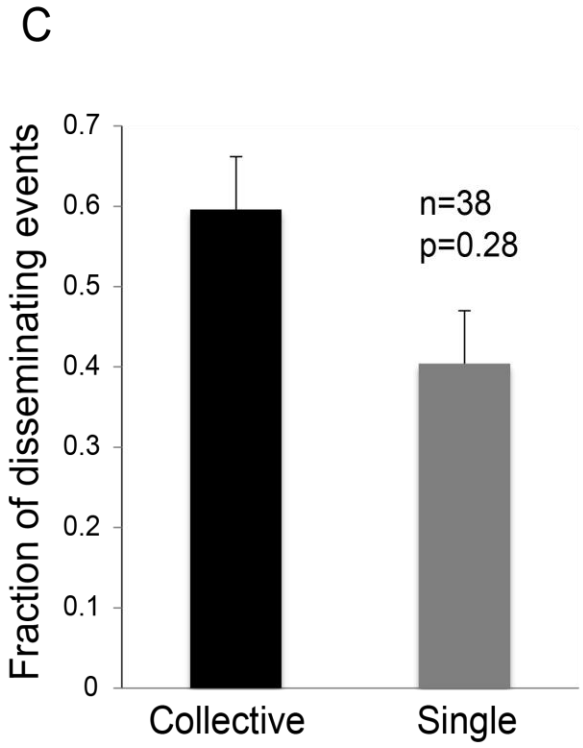
C
Fraction of disseminating events
0.7
0.6
0.5
0.4
0.3
0.2
0.1
0
n=38
p=0.28
Collective
Single

3.4 DIFFERENT MODES OF DISSEMINATION DRIVE OV90 METASTASIS *IN VIVO*

Next, I wanted to test whether collective or single cell dissemination occurs *in vivo*. As my project is looking at early metastatic steps, and mechanisms of cell detachment from primary tumors into suspension, I have decided to inject EOC cell directly into the ovary of mice. Contrary to injecting cell intra-peritoneally or sub-cutaneously, this technique allows for primary tumors to start in a clinically relevant environment, where cells can grow and disseminate into the abdomen. I have validated that this technique yields primary tumor growth, ascites formation, spheroid and single cell fraction in ascites and secondary tumors common to ovarian cancer patients (omentum, peritoneal lining, and pelvic organs).

Tracking the mode of metastasis was done by clonal analysis, where injected cells were labelled with either GFP or mCherry fluorescent dyes. Upon examination of disseminated spheroids in ascites, endogenous fluorescence informed of the dissemination mode. My experimental aims were twofold: 1) Quantify the frequencies of single and collective cell dissemination. 2) Quantify the frequency of cellular co-aggregation in ascites subsequent to dissemination.

For these experiments, mice were divided into two groups. The first group (Mixed) received a mixture of red and green cells in both ovaries. The second group (Separate) received red cells in one ovary and green cells in the other. In the Mixed group, if clusters in ascites are multi-colored, this indicates that clusters are polyclonal and arose from more than one cell, proving collective dissemination. Presence of single colored

clusters, which would be considered monoclonal, would support single cell dissemination. To address my second aim in the Separate group, if clusters were multi-colored, this would indicate that cells could aggregate into clusters in ascites, whereas single colored clusters indicates no mixing after dissemination (Figure 3.4.1).

Cells were homogenously mixed in a 50:50 red to green ratio in the Mixed group, and injected in both ovaries of each mouse. After generation of a mosaic tumor, the color combination observed in ascites spheroids and distant metastasis was used to extrapolate the mode of metastasis. To confirm the color distribution of primary and secondary tumors, wide-field tiling of whole tumor cryo-sections was done, confirming that in the Mixed group, mosaic primary and secondary tumors were obtained. In contrast, the Separate group tumors were found to be mainly single colored (Figure 3.4.2). Subsequently, ascites were drained, and cells were isolated. In addition, systemic blood was collected through cardiac puncture. Tumor cells were conveniently identifiable by their endogenous fluorescence in both ascites and collected blood. Interestingly, ascites spheroids were found to be 59% multicolored in the experimental group. When compared to the control group which bears only 19% of co-mixing, our data suggests that collective dissemination occurs *in vivo* as well, closely resembling data obtained from our 3D live-imaging (Figure 3.4.3). It is likely that the dual colored approach used here underestimates the real number of multicellular detachment events, because clusters of cells with all the same fluorescent marker may also detach together. In addition, 65% of CTM were found to exist as multicolored spheroids, suggesting that collectively disseminated cells are likely to maintain their cellular makeup even during haematogenous metastasis (Fig 3.4.4).

FIGURE 3.4.1. SCHEMATIC OVERVIEW OF OVARIAN ORTHOTOPIC INJECTIONS.

(A) Separate injections: each ovary was injected with OV90 cells that were labelled with as single fluorescent protein. Ascites spheroids and distant metastasis bear a single color.

(B) Mixed injections: each ovary was injected with a mix of green and red fluorescently-labelled cells. Ascites spheroids and distant metastasis have mosaic color labels of both red and green.

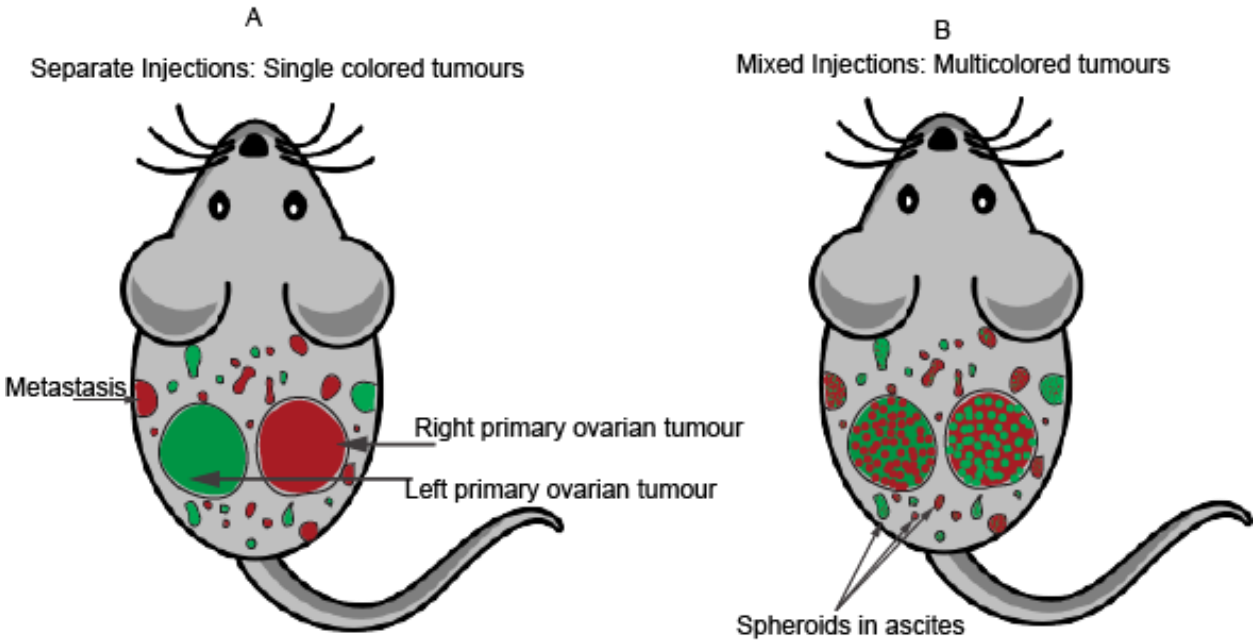
A
Separate Injections: Single colored tumours
Metastasis
Right primary ovarian tumour
Left primary ovarian tumour
B
Mixed Injections: Multicolored tumours
Spheroids in ascites

FIGURE 3.4.2. PRIMARY AND SECONDARY OVARIAN CANCERS EXHIBIT MOSAIC FLUORESCENT PATTERNS.

Cryo-sections of ovarian tumors and secondary metastasis in the Single group exhibit largely single colored fluorescence patterns, while the Mixed group cryo-sections exhibit largely multi-colored patterns of both red and green fluorescence in primary and secondary tumors. Scale bars = 200 μm.

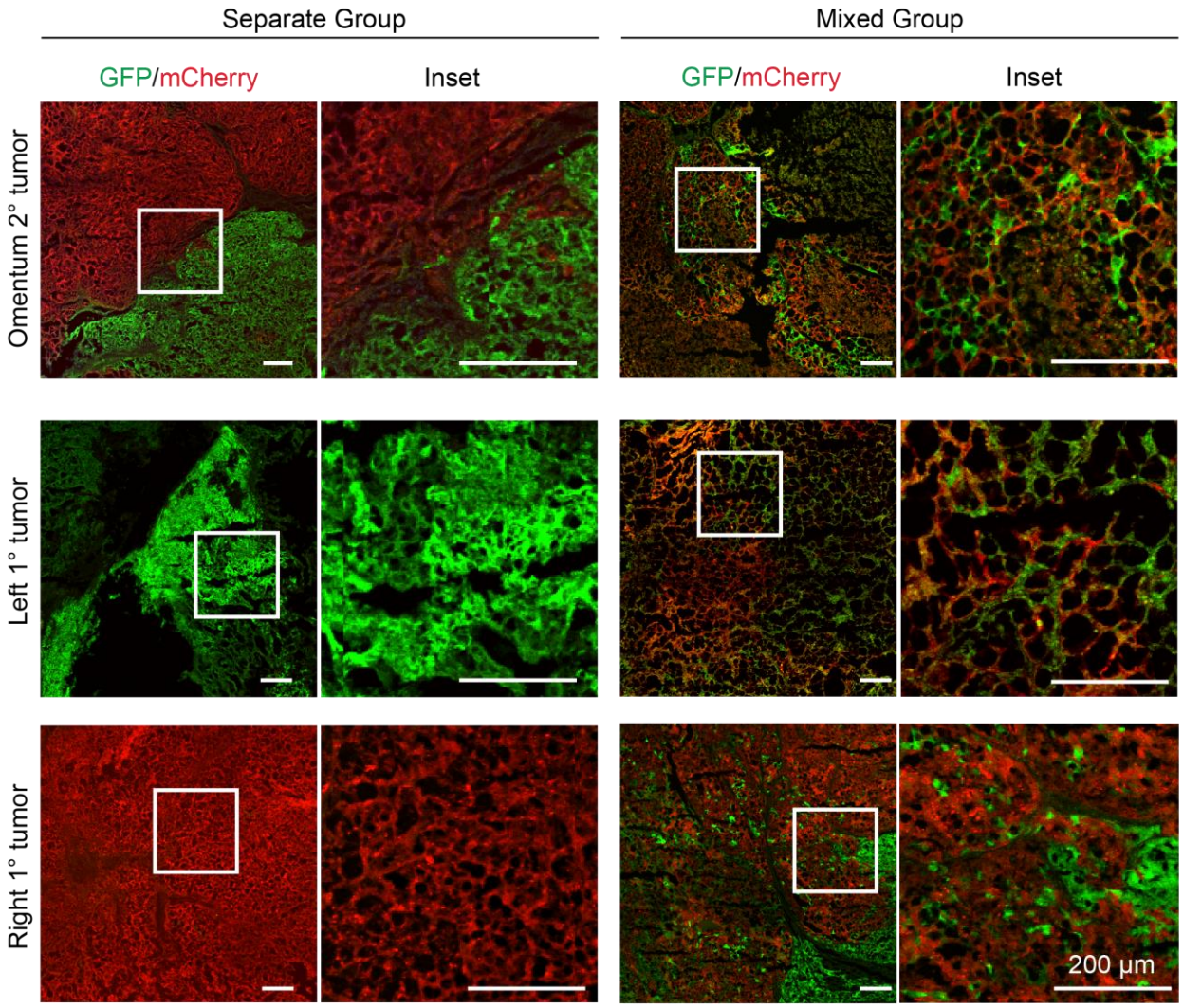
Separate Group
Mixed Group
GFP/mCherry
Inset
GFP/mCherry
Inset
Omentum 2° tumor
Left 1° tumor
Right 1° tumor
200 µm

FIGURE 3.4.3. MOUSE-DERIVED ASCITES CARRY OLIGOCLONAL SPHEROIDS

(A) Mouse-derived ascites from the single group are mainly single colored, whereas ascites from the mixed group are mostly multi-colored.

(B) Quantification of the percentage of ascites that are multicolored or single colored in both injections groups ($p<0.01$). N=4. Error bars represent standard error of means (SEM). Scale bar = 100 μm.

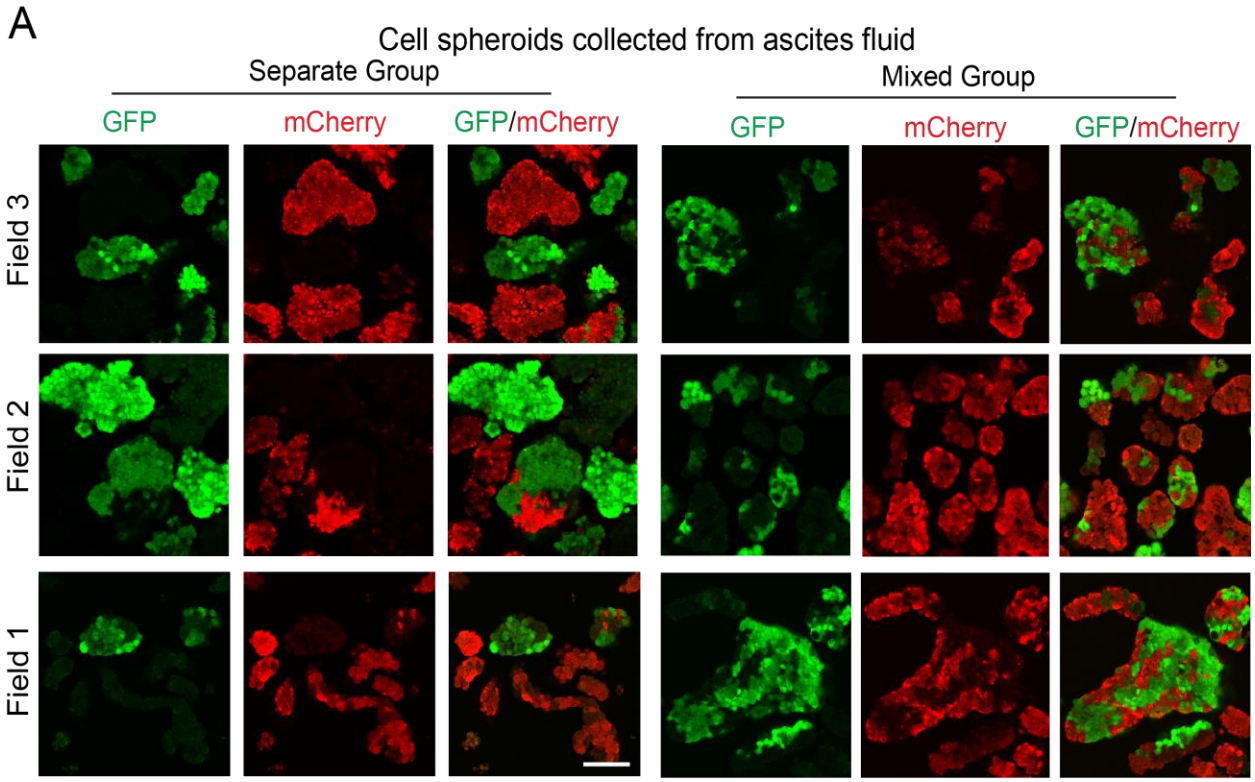
A
Cell spheroids collected from ascites fluid
Separate Group
Mixed Group
GFP
mCherry
GFP/mCherry
GFP
mCherry
GFP/mCherry
Field 3
Field 2
Field 1

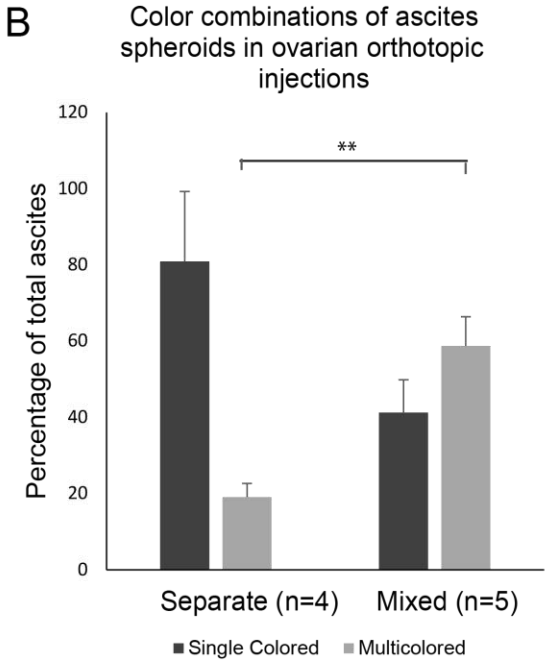
B
Color combinations of ascites spheroids in ovarian orthotopic injections
Percentage of total ascites
120
100
80
60
40
20
0
**
Separate (n=4)
Mixed (n=5)
Single Colored
Multicolored

FIGURE 3.4.4. MOUSE-DERIVED CTM CARRY OLIGOCLONAL SPHEROIDS.

(A) Mouse-derived CTM from the single group are mainly single colored, whereas ascites from the mixed group are mostly multi-colored.

(B) Quantification of the percentage of CTM that are multicolored or single colored in the separate injections group (N=1), or mixed injections group (N=4). Error bars represent SEM. Scale bar = 100 μm.

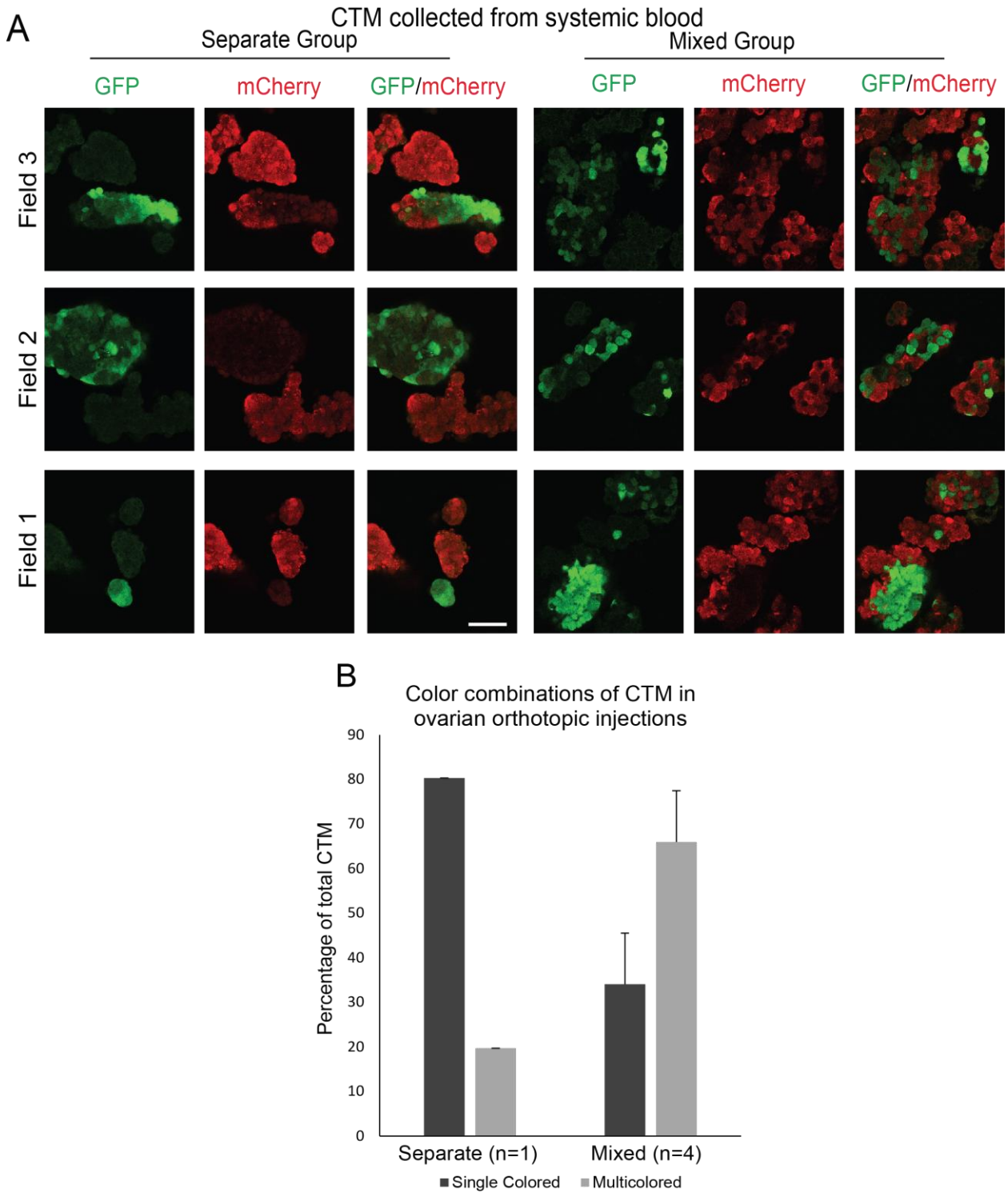
A
CTM collected from systemic blood
Separate Group
Mixed Group
GFP
mCherry
GFP/mCherry
GFP
mCherry
GFP/mCherry
Field 3
Field 2
Field 1
B
Color combinations of CTM in ovarian orthotopic injections
Percentage of total CTM
90
80
70
60
50
40
30
20
10
0
Separate (n=1)
Mixed (n=4)
Single Colored
Multicolored

3.5 ELUCIDATING THE INVOLVEMENT OF EMT IN OVARIAN CANCER DISSEMINATION

My results indicate that cells can disseminate as single cells or clusters *in vitro*, and that collective dissemination is likely the dominant event *in vivo*. Next I explored potential molecular mechanisms that may drive dissemination. EMT is one of the most widely studied mechanisms believed to control cancer cells' ability to migrate, invade and survive multiple challenges before seeding in a secondary site. However, some new studies are re-evaluating the necessity of EMT for metastasis [97]. I hypothesized that epithelial cell conversion to a mesenchymal phenotype may not be a limiting step for ovarian cancer dissemination, given that cells may collectively shed into the peritoneal cavity as clusters. EMT is a complex process, which not only affects cellular adhesion complexes, but also cellular dynamics, polarity, survival, stemness and motility [125]. To identify potential genes involved in promoting dissemination through EMT, I examined gene expression differences for adherent and detached cells using an EMT RT-qPCR profiler array that provides a transcriptional screening method for EMT related genes. The array's genes vary from exclusively epithelial genes, to EMT transcriptional regulators, and end with mesenchymal signature genes. RNA extraction was conducted on both attached OV90 cells from monolayers, and from DTCs collected from suspension media in triplicate. I found that the expression of MMP9, SNAI1, SNAI3, MSTR1 and EGFR were amongst genes that were significantly up-regulated in DTCs when compared to attached cells (2.93, 5.8 , 5.2 and 2.6 for EGFR, MMP9, SNAI1, and SNAI3 respectively) (Figure 3.5.1 and 3.5.2). EGFR (epidermal growth factor receptor) is a tyrosine kinase growth factor receptor rarely mutated in ovarian cancers. Despite overexpression of SNAI1, SNAI3 and MMP9 EMT promoter genes, both epithelial and

mesenchymal genes had no significant change, including E-cadherin (CDH1), N-cadherin (CDH2) and Vimentin. A full list of genes included in the array with average fold changes are represented in a heat map in Figure A2 (appendix). One interpretation of our results thus, may suggest that although EMT regulators, particularly SNAI1, may be involved in dissemination, it does not support that undergoing full EMT is necessary for dissemination. These results suggest that EMT regulators may be turned on in the cell machinery, not to switch to a mesenchymal phenotype as a direct aim, but rather might be regulating cellular survival and fitness.

FIGURE 3.5.1. DIFFERENTIAL EXPRESSION OF EMT MARKERS IN ATTACHED AND DISSEMINATED OV90 CELLS

RT-qPCR profiling of EMT markers in OV90 DTCs compared to OV90 monolayers as displayed in a volcano plot. Names highlighted in red in the upper right corner represent genes which are consistently upregulated in DTCs relative to attached cells ($p \leq 0.05$, N=3). Data was normalized using beta-2-microglobulin housekeeping gene (B2M).

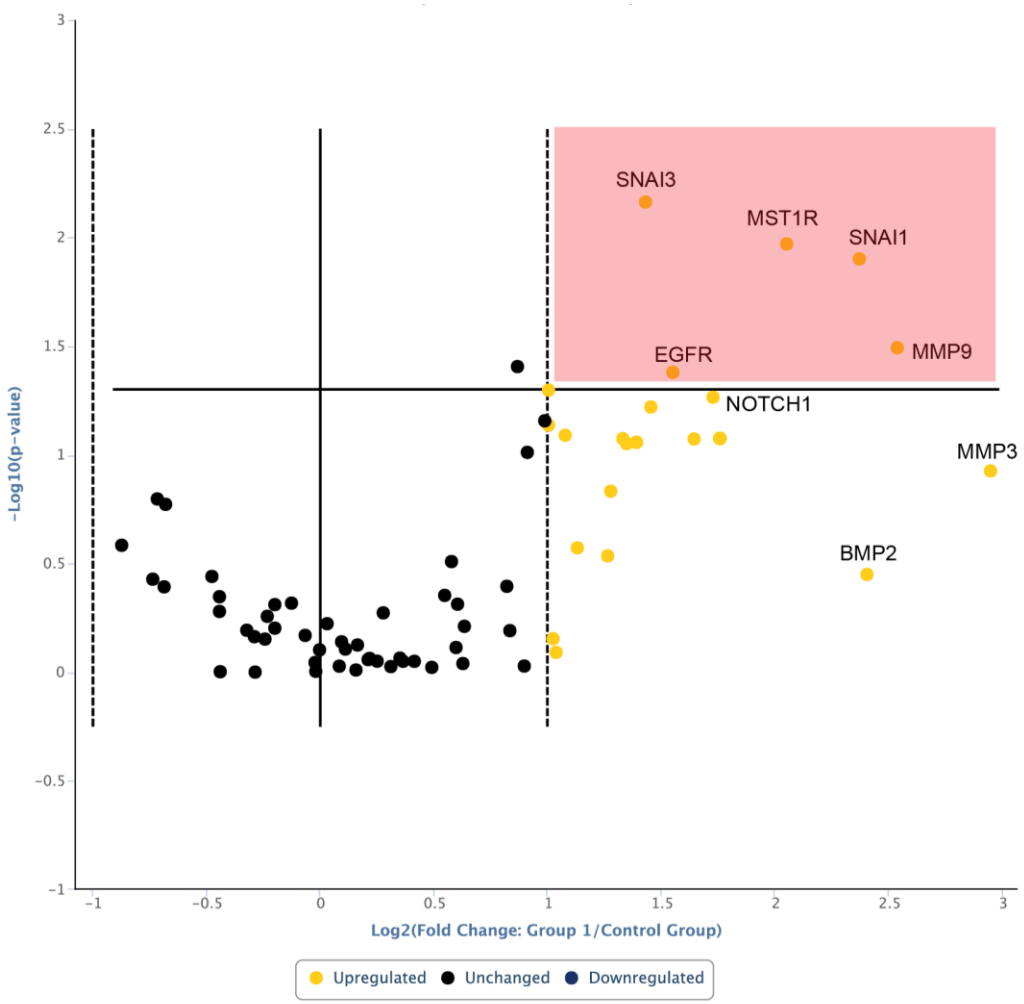
SNAI3
MST1R
SNAI1
MMP9
EGFR
NOTCH1
MMP3
BMP2
-Log10(p-value)
Log2(Fold Change: Group 1/Control Group)
Upregulated
Unchanged
Downregulated

FIGURE 3.5.2. DISSEMINATED OV90 CELLS EXHIBIT TRANSCRIPTIONAL UPREGULATION OF DISTINCT GENES.

RT-qPCR fold change quantification in the significantly upregulated genes in disseminated OV90 cells, compared to attached OV90 monolayers: EGFR, MMP9, SNAI1 and SNAI3 respectively. N=3. Error bars represent SEM.

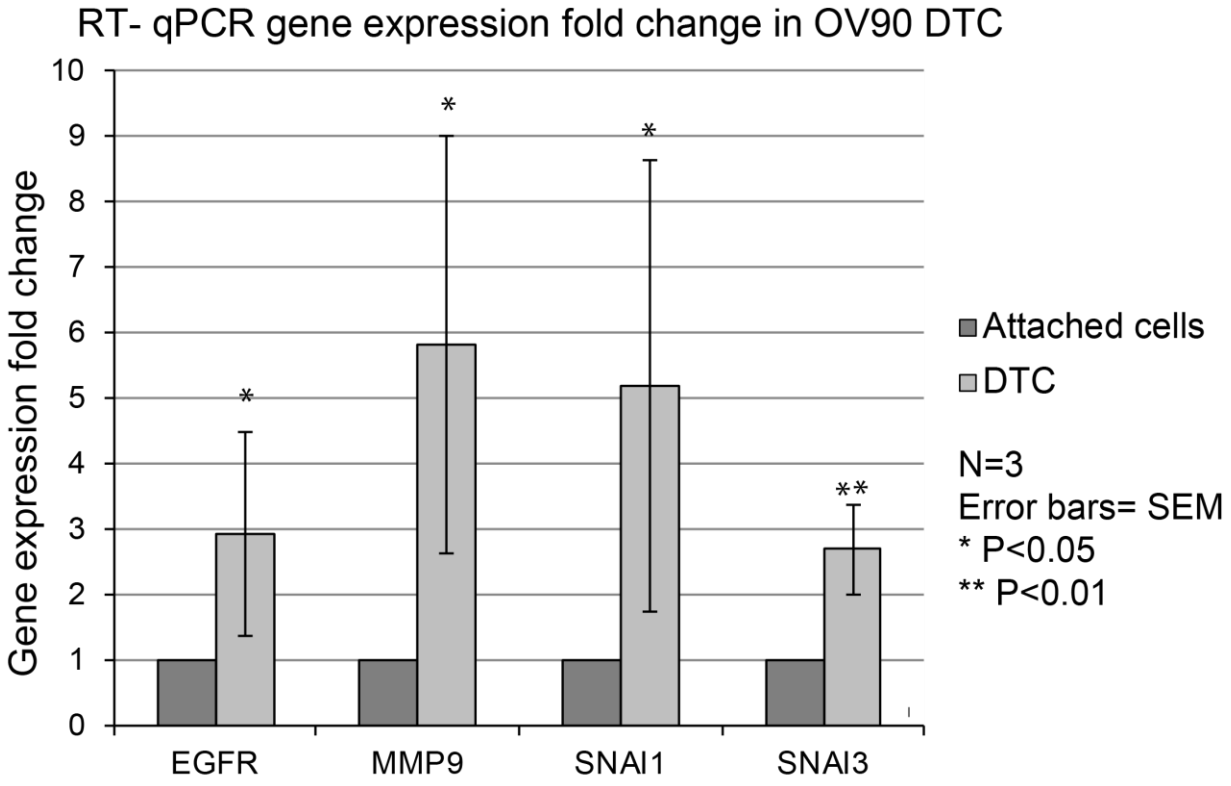
RT- qPCR gene expression fold change in OV90 DTC
Gene expression fold change
10
9
8
7
6
5
4
3
2
1
0
*
*
*
**
EGFR
MMP9
SNAI1
SNAI3
Attached cells
DTC
N=3
Error bars= SEM
* P<0.05
** P<0.01

3.6 EXPLORING DISSEMINATION DRIVERS IN OV90 CELLS

Following our observations that complete EMT is not be required for dissemination, we explored the possibility of dissemination being driven, promoted, or maintained by one of the following conditions: stem cell enrichment, cytoskeletal tension or matrix metalloproteinase activity.

Because MMP9 was significantly up-regulated in detached cells and it promotes cellular invasion [129], I asked whether MMP activity was necessary for detachment of EOC cells. To test the contribution of MMPs, I treated cultures with GM6001, a pan MMP blocker that inhibits MMP9, and compared the number and viability of disseminated cells to the vehicle control. I observed a 20% decrease in dissemination rates ($p<0.001$), coupled with approximately 8% reduction in survival rates of disseminated cells ($p<0.05$) (Figure 3.6.2). This indicates that MMPs have some role in dissemination, but may not be the primary driver.

Myosin-driven forces play a role in cytoskeletal re-arrangements, and was our last candidate to test in our panel using Blebbistatin and Rho kinase inhibitors (ROCK-I). RO enhances single cell egress from EOC spheroids [130], and malignant potential in soft matrices that resemble distant metastatic sites such as the omentum [131]. Upon treatment of cells with Blebbistatin and ROCK-I, dissemination rates dropped by 32% and 23%, respectively. In addition, viability rates were found to decrease to a striking 62% and 74% respectively (Figure 3.6.2).

Lastly, we hypothesized that a population of OV90 cells harbor stem cell characteristics of unlimited self-renewal and ability to survive in anchorage independent conditions,

which would be expected to amplify cellular survival in suspension in ascites. To test, this, OV90 and RH6 cells were seeded as single cells in low adhesion plates. Cells were later allowed to grow for 10-14 days, until monoclonal spheres were observed in suspension with a minimum diameter of 100 μm. As expected, RH6 cells did not yield any primary spheres upon initial seeding, reflecting their lack of tumorigenic ability. About 8% of OV90 cells were able to form primary spheres in OSE media. In addition, we have done the assay in conditions which can further support stem cell survival, including the usage of Mammocult (MC) base media, or OSE base media supplemented with FGF, EGF and Heparan sulfate (HS). MC is traditionally used to support mammary stem cell growth, however, sphere forming potential was only increased to 18%, with variable results that yielded a non-significant T-test score result. Consequently, we have hypothesized that using OSE media might be more suitable, however supported with stem cell growth promoters FGF, EGF and HS, which yielded a significantly increased sphere forming potential to 21% (Figure 3.6.1). Nonetheless, upon serial disaggregation and re-seeding of primary OV90 spheres, no cells were able to form secondary spheres under all three conditions, translating to weak self-renewal ability upon serial sphere formation tests. We concluded that stem cell populations were unlikely to be the main constituents of DTCs.

FIGURE 3.6.1. OV90 DTC COUNT AND VIABILITY *IN VITRO* IS AFFECTED BY MMPS AND MYOSIN DYNAMICS

(A) Quantification of OV90 DTC counts following drug treatment, normalized to vehicles. GM6001 (MMP inhibitor), Blebbistatin and RHOK-I (myosin inhibitors) drugs decrease the rate of dissemination in OV90 monolayers *in vitro*. Error bars represent SEM, N=4.

(B) Quantification of OV90 DTC viability following drug treatment, normalized to vehicles. GM6001 (MMP inhibitor), Blebbistatin and RHOK-I (myosin inhibitors) drugs decrease viability in OV90 monolayers *in vitro*. Error bars represent SEM, N=4.

A

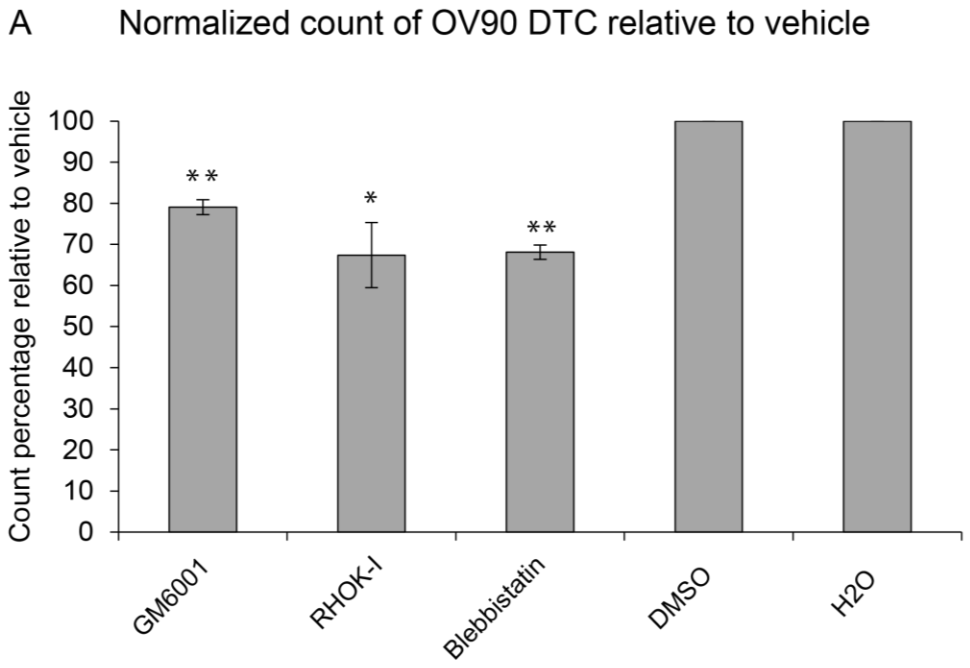

** P value <0.001
* P value = 0.052. Paired t-test.
N=4, error bars = SEM

B

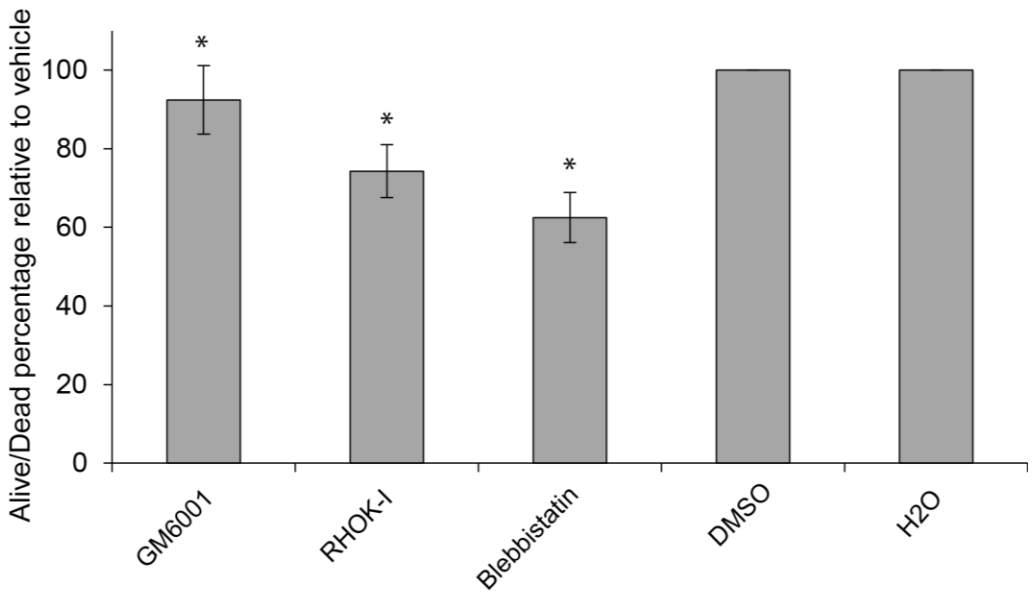

* P value < 0.05. Paired t-test.
N=5, error bars = SEM

FIGURE 3.6.2. EVALUATING STEM CELL CHARACTERISTICS IN OV90 CELLS.

OV90 cells are able to form monoclonal primary spheres with varying efficiencies in different growth conditions: OSE, Mammocult media (MC), or OSE media supplemented with EFG, FGF and HS (OSE+supplements). N=3

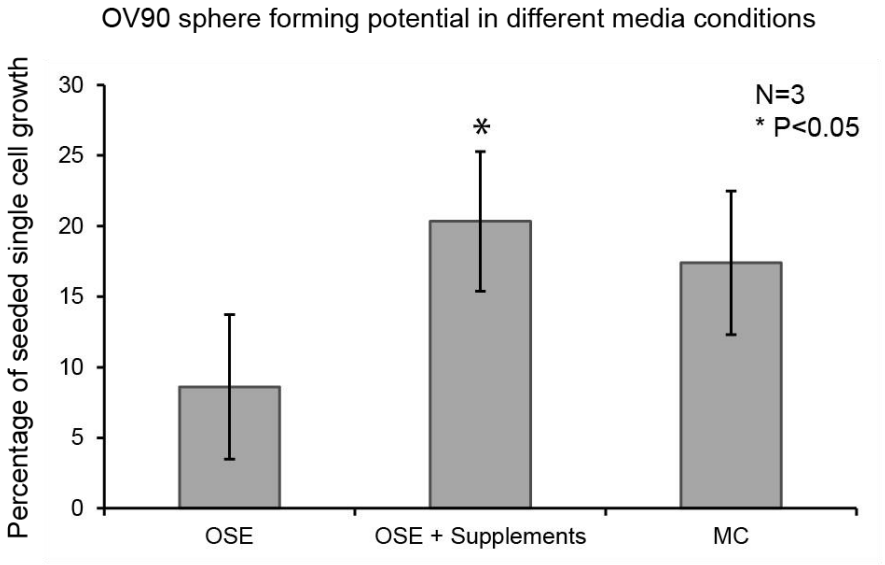

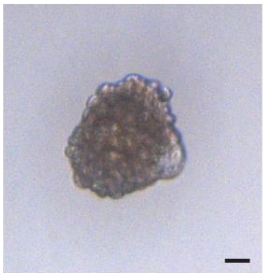

OV90 sphere in OSE media
Scale bar 50 µm

DISCUSSION, FUTURE DIRECTIONS AND CONCLUSIONS

DISCUSSION

4.1 SPHEROID FORMATION AND DISSEMINATION MODES

Non-metastatic tumors exhibit excellent 5-year survival rates in many cancer patients. However, localized disease is particularly rare for ovarian cancer patients, where most patients have metastatic disease that has extended beyond the primary site and regional lymph nodes. Alarmingly, the 5-year survival rate in patients with metastatic ovarian cancer has not changed in the 2015 reporting year compared to 2005 according to the US National Cancer Institute Surveillance, Epidemiology and End Results (SEER) registries [132, 133]. This data reflects the urgent need to advance our understanding of ovarian cancer metastasis, and to integrate metastatic colonization as a target for drug development. Multi-cellular ovarian cancer spheroid cells are consistently found in patient ascites, and have been found to not only contribute to metastasis, but also chemotherapy resistance through altered metabolism [134].

The mode of spheroid formation is largely un-investigated. I predict that spheroids may arise from four different models that depend on the metastatic time points and composition (Figure 4.1). While model 1 suggests that spheres may have a monoclonal origin, models 2 to 4 outline mechanisms through which polyclonal spheres may form: (1) Single cell dissemination from the primary tumor, followed by survival in ascites and proliferation into compact spheres can give rise to monoclonal units. (2) Single cell dissemination from the primary tumor, followed by survival in ascites, then mixing and

co-aggregating with other disseminated cells in suspension. (3) Collective dissemination, where a group of cells detach from the primary tumor together while maintaining their cell-cell interactions. Spheres may still co-aggregate with other cells in ascites. (4) Collective dissemination, where a sphere detaches from the primary tumor without co-aggregating with other disseminated cells in ascites.

FIGURE 4.1 OVERVIEW OF POSSIBLE DISSEMINATION MODES IN OVARIAN CANCER

Model 1

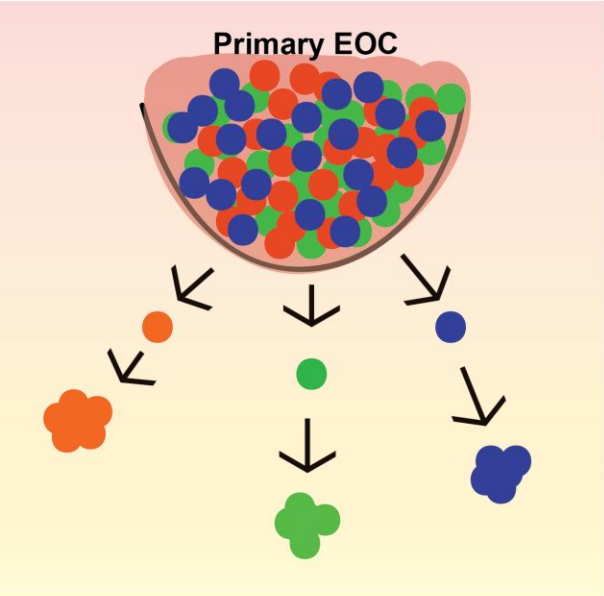

Model 2

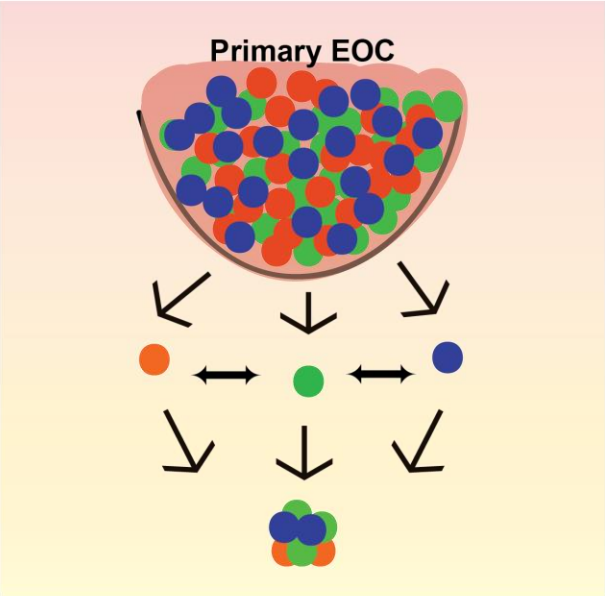

Model 3

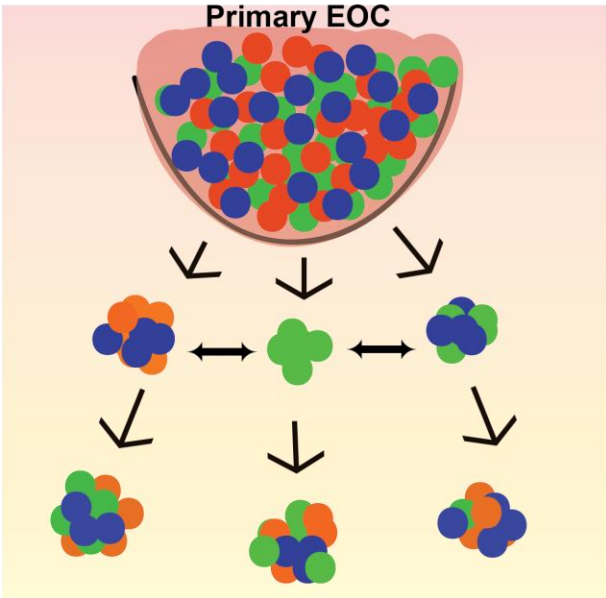

Model 4

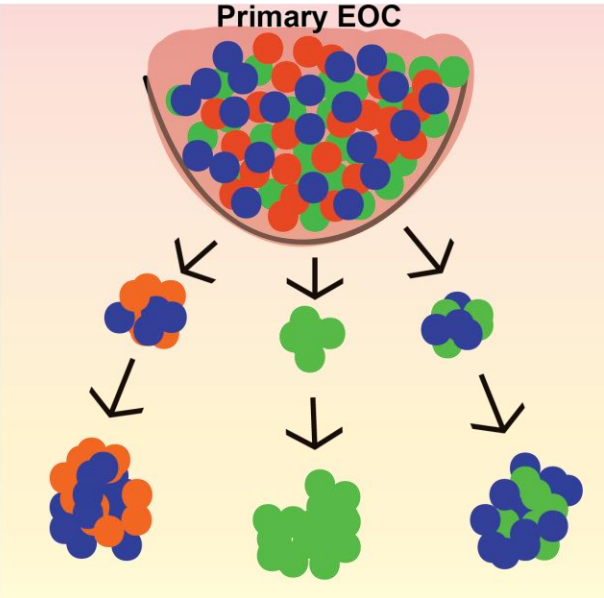

As it stands, an accepted view in the field adopts model 2, where spheroids arise from single cell dissemination followed by aggregation with other tumor cells [68]. Modest efforts were done to test if any of these models occurs *in vitro or in vivo*. Using OV90 cells, my data suggest that model 1 may not be efficient, as OV90 spheres have a survival rate of less than 10% as single cells in suspension in my *in vitro*, low attachment plate cultures. During viability analysis of disseminated cells in culture (Figure 3.2.1), I observed that dead cells (red) were often smaller in size than alive cells (green), supporting the notion that single cells have decreased survival potential in suspension compared to spheroids that were present in the same suspension. In the future, media manipulations of our sphere forming assay may reveal whether supplementation of particular cytokines, chemokines or growth factors may affect the survival of single cells. This assay can also be tested with additional EOC cell lines.

Following tumorsphere live imaging *in vitro*, and my *in vivo* results from the Mixed group of mice, I observed the occurrence of both model 1 and model 4. *In vitro* movies revealed that about 60% of dissemination events are collective, with the possibility of single cell dissemination to occur as well ($p=0.28$). In addition, clonal analysis from *in vivo* data suggests that similar trends are present as revealed by clonal analysis of spheroids in ascites. About 60% of spheroids were found to be multicolored (Figure 3.4.3), suggesting that groups of cells disseminated frequently from the primary mosaic tumor (Figure 3.4.2). My *in vivo* findings suggest that collective dissemination is at least as likely as single cell dissemination, as the possibility of multiple cells disseminating bearing the same color is foreseeable.

Ascites fluid usually needs a minimum of 1.5 L volume to be clinically detected at a sensitivity ranging between 50-94% [135]. While it contains a plethora of cellular components, largely consisting of immune and mesothelial cells, less than 0.1% is observed to contain cancer cells [136]. My data derived from the Separate injections group proposes that cellular co-aggregation (models 2 and 3) occurs only at the frequency of 20%, where multicolored spheroids were observed from primary tumors that were largely single colored. Taken together, I propose that model 4 might be the most frequent mode of dissemination, followed by model 1.

4.2 THE UNIQUE ENVIRONMENT OF OVARIAN CANCER

Collective dissemination has been previously shown to occur in breast cancer, where Aceto at al found that collectively disseminated cells have 23- to 50- fold increased metastatic potential compared to cells that underwent single cell dissemination [137]. Interestingly, single cells were at an advantage at the dissemination step in metastasis, as single cells were mechanically and physically more likely to invade through the basal lamina and endothelial barriers in breast cancer [138, 139]. Despite clusters being at a disadvantage in this step, they had increased efficiency in subsequent steps involving survival under the sheer stress in circulation [138, 139]. As clusters retain cell-cell interactions, cells may evade anoikis before arresting in a perivascular niche, or implanting at a distant site, giving them an overall increased efficiency in colonizing compared to single cells [63]. In my *in vitro* and *in vivo* data, single and collective dissemination events occurred at relatively equal frequencies, with some data

suggesting that collective dissemination might be more efficient for later survival. The differences we observe can be attributed to the essentially divergent environments of ovarian cancer, and solid epithelial cancers such as breast cancer. Whereas both cancers in question are epithelial, ovarian cancer cells need to go through a different course to colonize. This is exemplified by the dispensable breach of basement membranes and endothelial barriers, both at the departure step from the primary tumor, and at the entry step at the secondary site [8]. In addition, disseminated cells do not undergo the same stress forced by the circulation in other cancer types while in transit. Ovarian cells may get exfoliated from the primary tumor, where they may remain in suspension, or attach to the mesothelial lining of the abdomen [66]. Taken together, ovarian cancer cells do face a fundamentally different set of challenges than most epithelial cancers. In a clinical context, many disseminated cells face anchorage independent conditions, in addition to chemotherapeutic agents. I therefore propose that retaining cell-cell interactions in spheroids helps cells escape anoikis and proliferate before colonizing to distant sites. In addition, spheroids exhibit reduced drug penetration [110], which may occur through physical shielding of outer cells in favor of inner core cells.

4.3 EPITHELIAL MESENCHYMAL TRANSITION AND OVARIAN CANCER METASTASIS

To investigate the roles of EMT, we have chosen epithelial cells for our project, to represent the starting point of EOC. As epithelial characteristics were found to be exhibited in both primary and secondary sites in EOC [104, 122], starting with epithelial

cells will allow phenotypical examination coupled with metastasis. Our 2D cultures of OV90 and OVCAR3 cells demonstrate strong expression of E-cadherin and ZO-1, with negative expression of Vimentin. Reverse trends were found in RH6 cell, interestingly, as their mesenchymal phenotype is coupled with their lack of tumorgenecity [123].

EMT is traditionally thought to drive cellular invasion and metastasis, however the exact role and defining features of EMT are under debate. While over expression of EMT factors SNAIL and ZEB1 may be a part of the process, overt EMT is also coupled with down-regulation of epithelial markers (E-cadherin and cytokeratins), and up-regulation of mesenchymal markers (such as Vimentin). In the complexity of these pathways, EMT can be described as a spectrum, where different levels of epithelial, mesenchymal, or regulator genes can generate variable states [124]. In addition, cells may undertake inter-conversions along the epithelial-mesenchymal axis, resulting in a state of plasticity that is often advantageous to cancer spread. Acquiring a transiently mesenchymal state may enhance departure form primary sites and increase invasiveness of epithelial cancers, particularly during dissemination and colonization of distant sites. In context of ovarian cancer, my data argues that OV90 cells are able to disseminate while maintaining their E-cadherin expression and lack of vimentin. While ovarian cancer cells have less barriers to invade through, cellular attachment to the primary tumor remains a hurdle for epithelial cells to overcome to undergo separation. In the presence of MMPs, such as MMP9, epithelial cells may be able to efficiently detach by degrading surrounding matrix. In addition, regulation of cortical cell tension while undergoing dissemination may play a vital role in not increasing the efficiency of detachment, but also cell viability following the event. It has been reported upon myosin inhibition in later

time points following dissemination, that ROCK-activity enhances single cell egress from EOC spheroids [130], and malignant potential in soft matrices that resemble distant metastatic sites such as the omentum [131].

Overt EMT might however be needed for chemoresistance, as a recent report suggests that EMT is not needed for metastasis, but does promote chemoresistance in breast cancer [97].

4.4 ROLES OF HETEROGENEITY IN SNAI1 AND ZEB1 LOCALIZATION AND EXPRESSION

Although epithelial states are maintained following dissemination in my data (Figure 3.5.2), some EMT factors were up regulated (SNAI1, SNAI3). Interestingly, mosaic levels of both SNAI1 and ZEB1 were seen in 2D culture, coupled with E-cadherin expression. This phenotype can be explained by a plastic state, where cells have a hybrid of epithelial and EMT markers expressed. A heterogeneity is observed in the levels of expression and subcellular localization, which might be dependent on cellular density. I propose that EMT factors SNAI1 and ZEB1 might be inducing partial EMT, to enhance tumor dissemination and survival, while retaining epithelial phenotypes. In addition to promoting cellular stemness, survival, chemo-resistance and dormancy [126, 127, 140-142], EMT factors might be down-regulating cellular adhesions to allow for dissemination. In one example where tumorspheres were immune-fluorescently stained, I observed a spheroid expressing nuclear ZEB1 with varying levels (Figure 4.2). Interestingly, E-cadherin was retained with the exception of a few cells at the edge of a

sphere, where ZEB1 had relatively high expression. While further analysis and staining needs to be done to fully accept this as a mechanism, this data suggests that E-cadherin might only need to be down-regulated partially in a metastatic unit, while different thresholds of ZEB1 control the epithelial phenotype. ZEB1 has been reported to operate in a dose-dependent manner, where low levels of ZEB1 were sufficient for tumor initiation, however higher levels were required for inducing metastasis [143].

FIGURE 4.2: MOSAIC E-CADHERIN EXPRESSION IN OV90 TUMORSPHERES

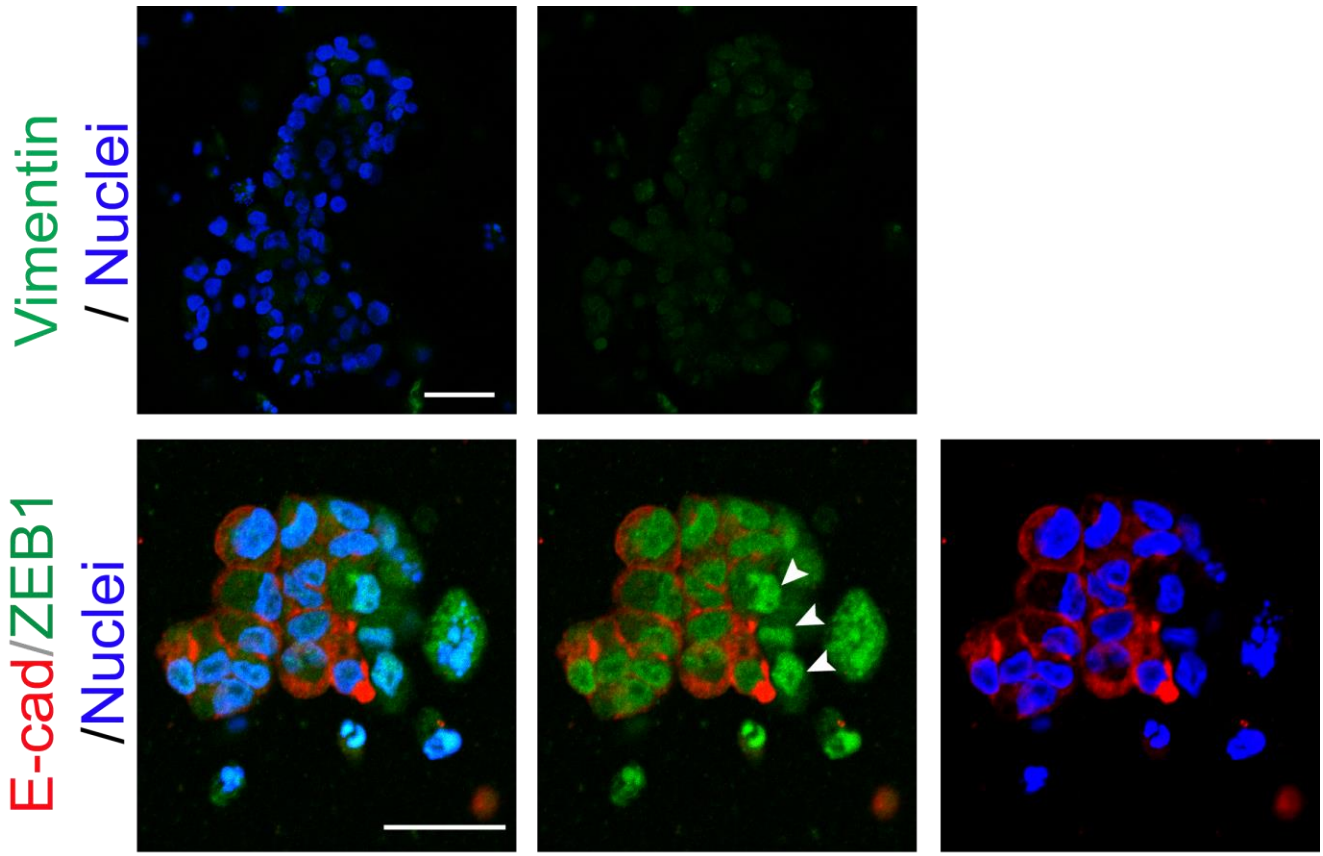
Vimentin
/ Nuclei
E-cad/ZEB1
/Nuclei

Our finding of cytoplasmic ZEB1 and SNAI1 might indicate that these EMT factors may be under the regulation of further factors, as they are most known of their transcriptional repressive activity of E-cadherin in the nucleus [77, 144]. Our observation that ZEB1 localization may vary with cellular density (Figure 3.1.5) may be related with the recent finding of a direct interaction between ZEB1, and the Hippo pathway effector Yes associated protein (YAP1) in breast cancer cells [145]. The Hippo pathway plays a major role in regulating cellular survival, stemness and apoptosis in normal tissue homeostasis and in cancerous tissues. As a transcriptional co-activator, YAP plays a major role in the pathway by helping induce the transcription of proliferative genes, and was reported to be an oncogene in ovarian cancer [146]. Interestingly, YAP and ZEB1 exhibit a common behavior of localizing to the nucleus in sparse culture, but in the cytoplasm with increased cellular densities [147]. The recent finding of YAP1 and ZEB1 directly interacting and sharing a set of target genes to induce [145], supports future investigation on whether ZEB1 has additional functions, possibly in the cytoplasm, which can regulate cellular transformation in ovarian cancer.

SNAI1 has been reported to vary in localization [148], where glycogen synthase kinase 3-beta (GSK-3β) phosphorylation can favor its nuclear export and target SNAI1 for degradation [149], while other groups have found that phosphorylation by p21 activated kinase (Pak1) and protein kinase D1 (PKD1) may induce its nuclear import [150, 151]. While little is known about GSK-3β contribution in ovarian cancer, it is possible that cytoplasmic SNAI1 in 2D cultures is being targeted for degradation. GSK-3β regulation might be occurring upon dissemination, leading to accumulation of SNAI1 in disseminated cells where it can affect cell survival and migration. For example, the

PI3K-AKT pathway is activated in approximately 70% of ovarian cancer and is implicated in chemotherapy resistance [30]. PI3K-AKT has been shown to inhibit SNAI1 phosphorylation by GSK-3β [125], making it a candidate mechanism to stabilize SNAI1.

4.5 EXPLORING DISSEMINATION DRIVERS

While MMPs were reported to contribute to spheroid formation [129], MMP9 in particular predicts decreased survival of OvCa patients [152]. Proteinases are crucial for ascites pathogenesis, catalyzing migration and invasion through the mesothelial lining in the abdominal cavity. My data demonstrate that MMP9 expression was significantly up-regulated in detached cells relative to attached cells, suggesting it may facilitate detachment in presence of intact E-cadherin. Indeed, blocking MMP activity with a broad MMP inhibitor reduced DTC count and viability in culture (Figure 3.6.1). Whether this is specific to MMP9, or involved other MMPs require additional studies. However, my studies showed that inhibiting MMPs did not completely abrogate detachment, indicating that it has a minor contribution, or other proteinases are involved that were not detected in the gene expression array or are not targeted by the inhibitor used. Further testing of additional proteinases through immunoblot and knockdown studies in the future would resolve potential roles for specific MMPs in detachment.

In addition to SNAI1, SNAI3 and MMP9, EGFR was up-regulated in DTCs. EGFR, a SNAI1 inducer [126], has interestingly been correlated with decreased OvCa patient survival, and might be involved in regulating OvCa cell survival following detachment from primary tumor [153]. While our RT-qPCR array provided candidates which may be

regulating dissemination, gene hits will need to be further characterized functionally and by testing their protein expression levels in DTCs compared to attached cells.

Our earlier hypothesis that mitosis could contribute to dissemination will require further investigation. Mitosis might help reduce cell adhesions as cells round up in a form susceptible to detachment (Figure 3.3.1). In addition, mis-oriented cell divisions could lead to the release of daughter cells from the epithelium. However, none of the detaching cells captured by video *in vitro* did so after a mitotic event. Furthermore, no mitotic cells detached, and all divisions were in the plane of epithelium. However, the number of visible mitotic cells evaluate was low, and further investigation necessary before fully excluding this as a mechanism of dissemination. Nonetheless, my data indicate that mitotic events unlikely contribute as a major mechanism for cell detachment.

FUTURE DIRECTIONS

My data strongly support a model in which groups of ovarian cancer cells can detach, leading to the cell clusters that are frequently observed in ovarian cancer patients. There are several exciting avenues that this work can be further extended. First, providing direct evidence that EOC indeed detach as groups of cells *in vivo* would further determine the frequency and relative importance of this mode of dissemination. This would best be achieved using *in vivo* live imaging with multiple EOC cell lines. To this end, I have devised a live-imaging system to allow visualization of disseminating cells *in vivo*. To do this, a coverglass secured in a titanium window was stitched to the

lateral side of the animal's abdomen after ascites drainage (Figure 4.3 A). While under anesthesia, the mouse was fixed on the stage of a ZEISS confocal microscope, and fluorescence is visualized through the coverglass. I have successfully installed the window in pilot trials, where fluorescent mammary 4T1 cancer cells were injected in the ovary. Preliminary imaging results demonstrated the mosaic fluorescence of the tumor (Figure 4.3 B), however imaging will need to be optimized over extended periods of time to be able to visualize individual cell movement. Results from such a system will be novel in the literature to visualize ovarian cancer cell dissemination in real time.

FIGURE 4.3: INSTALLATION OF OVARIAN IMAGING WINDOW

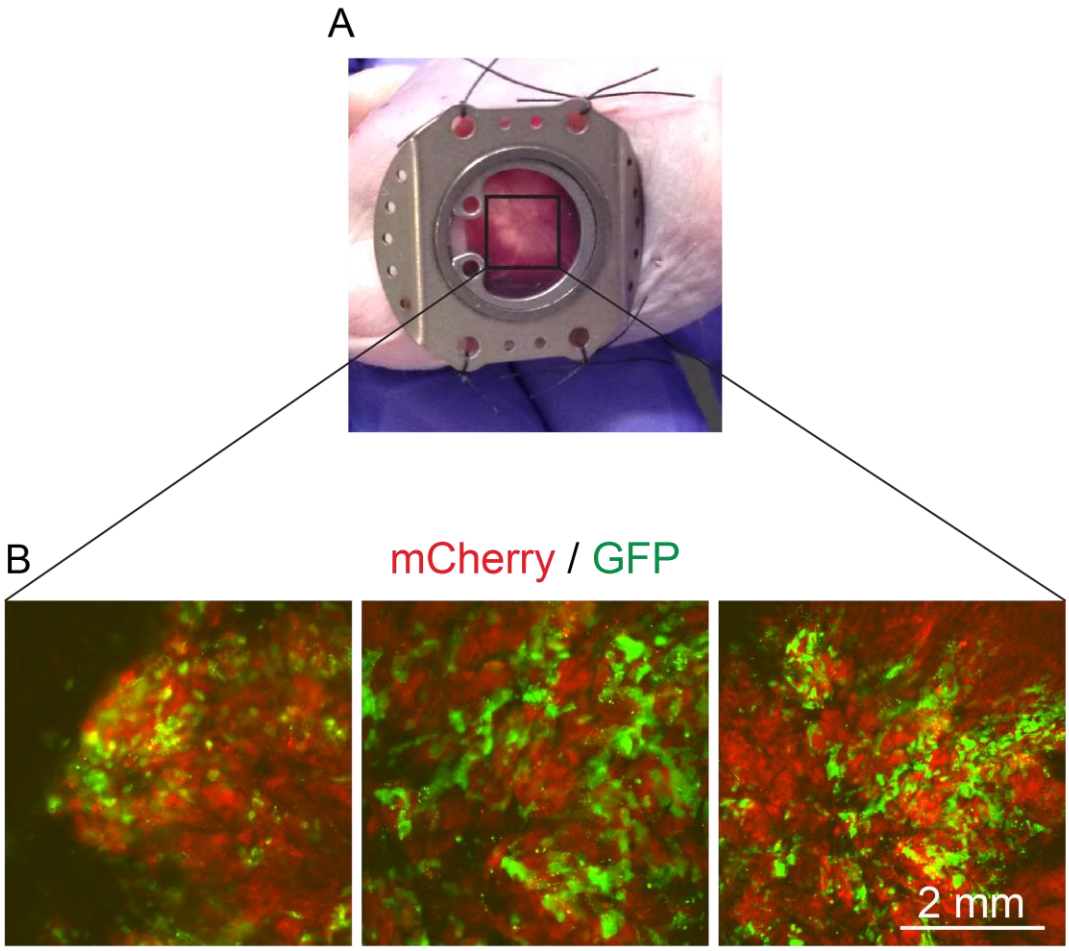
A
B
mCherry / GFP
2 mm

Further molecular and functional characterization is needed to investigate the exact role of several EMT transcription factors in single cell and collective dissemination. This could be done by knocking down expression of ZEB1 and SNAI1 in cells and examining the effect on mode of dissemination and metastasis. Short hairpin RNAs for transcriptional degradation, or genetic knock out using the CRISPR/Cas9 system, could be used and we predict that ZEB1/SNAI1 knock down/out will be decrease dissemination and metastatic colonization if they are required for detachment or survival.

It is possible that EMT is transient or occurs in a subpopulation of cells that are difficult to detect. To test the general requirement for EMT we could inhibit EMT by expressing a miR200-casette that has been shown to block EMT [154]. This would lock cells in an epithelial phenotype and we could asses the mode of dissemination and efficiency of metastasis. Meeting the challenge of ascites plasticity, particularly along the EMT axis, should also be addressed. Disseminated tumor cells may undergo rapid reversible changes in expression of EMT regulators, a characteristic difficult to capture as harvested samples are only looked at for a specific time frame. We are thus in the process of developing an EMT biosensor, in collaboration with Dr. Peter Siegel, that labels cells with a permanent fluorescent marker upon entering an EMT program. Using EMT regulators' promoters to express Cre, activation of an EMT program will trigger excision of a stop codon controlling a fluorescent dye, making this effect permanent even if cells undergo MET. This system would help us determine whether the epithelial phenotype we predict to find in ascites was permanent, or whether cells underwent EMT transiently at any point in time. It is acknowledged that cancer cells exhibit various

modes of migration as individual or groups of cells [155], where the cytoskeleton can drive actin-rich protrusions in an elongated cell shape. Alternatively, highly contractile actomyosin forces can result in a more rounded cell shape during cell migration, also known as an amoeboid state [156]. Despite both modes depending on a plethora of distinct kinases, GTPases, matrix proteinases and other molecular drivers [156], interconversions between migration states have previously been reported [157]. While OV90 and OVCAR3 cells primarily exhibit more epithelial than rounded characteristics when compared to a panel of ovarian cancer cells [158], exploring the possibility of epithelial to amoeboid transition in correlation to changes in genetic and proteomic expression profiles following dissemination *in vivo* will deepen our understanding of the plastic spectrum of states ovarian cancer cells experience.

Although OV90 cells may not seem to rely on stem cell enrichment for dissemination, additional multiple factors may be regulating cell survival and colonization. Validating our *in vitro* and *in vivo* results with additional epithelial cell lines, such as OVCAR3, and patient-derived primary ascites, will help us find pathways that are indispensable for ovarian metastasis and spheroid formation.

CONCLUSION

Based on my data presented here, I propose the following model, which drives dissemination and spheroid formation in ovarian cancer. Groups of cells may detach collectively from primary tumors, in the absence of junction dissolution and complete EMT. Spheroids formed by this model are metastatically competent, and infrequently mix with other spheroids.

My data helps better understand how spheroids arise, and sets a foundation to study how cell-cell interactions in spheroids can be exploited as a therapeutic target to decrease their malignancy. Mapping out the mechanisms underlying collective dissemination will impact clinical approaches used to alleviate ascites symptoms and limit metastatic colonization.

BIBLIOGRAPHY

1. Auersperg, N., et al., *Ovarian surface epithelium: biology, endocrinology, and pathology.* Endocr Rev, 2001. **22**(2): p. 255-88.
2. Kobayashi, A. and R.R. Behringer, *Developmental genetics of the female reproductive tract in mammals.* Nat Rev Genet, 2003. **4**(12): p. 969-80.
3. Auersperg, N., et al., *The biology of ovarian cancer.* Semin Oncol, 1998. **25**(3): p. 281-304.
4. Fathalla, M.F., *Factors in the causation and incidence of ovarian cancer.* Obstet Gynecol Surv, 1972. **27**(11): p. 751-68.
5. Cannistra, S.A., *Cancer of the ovary.* N Engl J Med, 2004. **351**(24): p. 2519-29.
6. George, S.H., A. Milea, and P.A. Shaw, *Proliferation in the normal FTE is a hallmark of the follicular phase, not BRCA mutation status.* Clin Cancer Res, 2012. **18**(22): p. 6199-207.
7. Gaytan, F., et al., *Differential effects of RU486 and indomethacin on follicle rupture during the ovulatory process in the rat.* Biol Reprod, 2003. **69**(1): p. 99-105.
8. Ng, A. and N. Barker, *Ovary and fimbrial stem cells: biology, niche and cancer origins.* Nat Rev Mol Cell Biol, 2015. **16**(10): p. 625-38.
9. Fathalla, M.F., *Incessant ovulation--a factor in ovarian neoplasia?* Lancet, 1971. **2**(7716): p. 163.

10. Scully, R.E., *Early de novo ovarian cancer and cancer developing in benign ovarian lesions.* Int J Gynaecol Obstet, 1995. **49 Suppl**: p. S9-15.
11. Auersperg, N., *Ovarian surface epithelium as a source of ovarian cancers: unwarranted speculation or evidence-based hypothesis?* Gynecol Oncol, 2013. **130**(1): p. 246-51.
12. Ahmed, N., K. Abubaker, and J.K. Findlay, *Ovarian cancer stem cells: Molecular concepts and relevance as therapeutic targets.* Mol Aspects Med, 2014. **39**: p. 110-25.
13. Jazaeri, A.A., et al., *Molecular requirements for transformation of fallopian tube epithelial cells into serous carcinoma.* Neoplasia, 2011. **13**(10): p. 899-911.
14. Karst, A.M., K. Levanon, and R. Drapkin, *Modeling high-grade serous ovarian carcinogenesis from the fallopian tube.* Proc Natl Acad Sci U S A, 2011. **108**(18): p. 7547-52.
15. Prat, J. and F.C.o.G. Oncology, *Staging classification for cancer of the ovary, fallopian tube, and peritoneum.* Int J Gynaecol Obstet, 2014. **124**(1): p. 1-5.
16. Tavassoli, F. and P. Devilee, *Tumors of the ovary and peritoneum. Tumors of the Breast and Female Genital Organs. Edited by P Kleihues and L Sobin*. 2003, Lyon, France, IARC Press.
17. Piek, J.M., et al., *Dysplastic changes in prophylactically removed Fallopian tubes of women predisposed to developing ovarian cancer.* J Pathol, 2001. **195**(4): p. 451-6.
18. Kindelberger, D.W., et al., *Intraepithelial carcinoma of the fimbria and pelvic serous carcinoma: Evidence for a causal relationship.* Am J Surg Pathol, 2007. **31**(2): p. 161-9.
19. Medeiros, F., et al., *The tubal fimbria is a preferred site for early adenocarcinoma in women with familial ovarian cancer syndrome.* Am J Surg Pathol, 2006. **30**(2): p. 230-6.
20. Seidman, J.D., P. Zhao, and A. Yemelyanova, *"Primary peritoneal" high-grade serous carcinoma is very likely metastatic from serous tubal intraepithelial carcinoma: assessing the new paradigm of ovarian and pelvic serous carcinogenesis and its implications for screening for ovarian cancer.* Gynecol Oncol, 2011. **120**(3): p. 470-3.
21. Mehrad, M., et al., *A pathologist's road map to benign, precancerous, and malignant intraepithelial proliferations in the fallopian tube.* Adv Anat Pathol, 2010. **17**(5): p. 293-302.
22. Kuhn, E., et al., *TP53 mutations in serous tubal intraepithelial carcinoma and concurrent pelvic high-grade serous carcinoma--evidence supporting the clonal relationship of the two lesions.* J Pathol, 2012. **226**(3): p. 421-6.
23. Przybycin, C.G., et al., *Are all pelvic (nonuterine) serous carcinomas of tubal origin?* Am J Surg Pathol, 2010. **34**(10): p. 1407-16.
24. Singer, G., et al., *Mutations in BRAF and KRAS characterize the development of low-grade ovarian serous carcinoma.* J Natl Cancer Inst, 2003. **95**(6): p. 484-6.
25. Shih Ie, M. and R.J. Kurman, *Ovarian tumorigenesis: a proposed model based on morphological and molecular genetic analysis.* Am J Pathol, 2004. **164**(5): p. 1511-8.
26. Gershenson, D.M., et al., *Clinical behavior of stage II-IV low-grade serous carcinoma of the ovary.* Obstet Gynecol, 2006. **108**(2): p. 361-8.
27. Lengyel, E., *Ovarian cancer development and metastasis.* Am J Pathol, 2010. **177**(3): p. 1053-64.

28. Kinzler, K.W. and B. Vogelstein, *Lessons from hereditary colorectal cancer.* Cell, 1996. **87**(2): p. 159-70.
29. Hsu, C.Y., et al., *Characterization of active mitogen-activated protein kinase in ovarian serous carcinomas.* Clin Cancer Res, 2004. **10**(19): p. 6432-6.
30. Bast, R.C., Jr., B. Hennessy, and G.B. Mills, *The biology of ovarian cancer: new opportunities for translation.* Nat Rev Cancer, 2009. **9**(6): p. 415-28.
31. Cheng, J.Q., et al., *AKT2, a putative oncogene encoding a member of a subfamily of protein-serine/threonine kinases, is amplified in human ovarian carcinomas.* Proc Natl Acad Sci U S A, 1992. **89**(19): p. 9267-71.
32. Shayesteh, L., et al., *PIK3CA is implicated as an oncogene in ovarian cancer.* Nat Genet, 1999. **21**(1): p. 99-102.
33. Kipps, E., D.S. Tan, and S.B. Kaye, *Meeting the challenge of ascites in ovarian cancer: new avenues for therapy and research.* Nat Rev Cancer, 2013. **13**(4): p. 273-82.
34. Tomao, F., et al., *Current status of bevacizumab in advanced ovarian cancer.* Onco Targets Ther, 2013. **6**: p. 889-99.
35. Zhan, N., W.G. Dong, and J. Wang, *The clinical significance of vascular endothelial growth factor in malignant ascites.* Tumour Biol, 2015.
36. Aghajanian, C., et al., *Final overall survival and safety analysis of OCEANS, a phase 3 trial of chemotherapy with or without bevacizumab in patients with platinum-sensitive recurrent ovarian cancer.* Gynecol Oncol, 2015. **139**(1): p. 10-6.
37. Ahmed, N. and K.L. Stenvers, *Getting to know ovarian cancer ascites: opportunities for targeted therapy-based translational research.* Front Oncol, 2013. **3**: p. 256.
38. Tan, D.S., R. Agarwal, and S.B. Kaye, *Mechanisms of transcoelomic metastasis in ovarian cancer.* Lancet Oncol, 2006. **7**(11): p. 925-34.
39. Ahmed, N., et al., *Ascites induces modulation of alpha6beta1 integrin and urokinase plasminogen activator receptor expression and associated functions in ovarian carcinoma.* Br J Cancer, 2005. **92**(8): p. 1475-85.
40. Ahmed, N., et al., *Integrin-linked kinase expression increases with ovarian tumour grade and is sustained by peritoneal tumour fluid.* J Pathol, 2003. **201**(2): p. 229-37.
41. Mills, G.B., et al., *Ascitic fluid from human ovarian cancer patients contains growth factors necessary for intraperitoneal growth of human ovarian adenocarcinoma cells.* J Clin Invest, 1990. **86**(3): p. 851-5.
42. Mills, G.B., et al., *A putative new growth factor in ascitic fluid from ovarian cancer patients: identification, characterization, and mechanism of action.* Cancer Res, 1988. **48**(5): p. 1066-71.
43. Strobel, T., L. Swanson, and S.A. Cannistra, *In vivo inhibition of CD44 limits intra-abdominal spread of a human ovarian cancer xenograft in nude mice: a novel role for CD44 in the process of peritoneal implantation.* Cancer Res, 1997. **57**(7): p. 1228-32.
44. Gardner, M.J., et al., *Human ovarian tumour cells can bind hyaluronic acid via membrane CD44: a possible step in peritoneal metastasis.* Clin Exp Metastasis, 1996. **14**(4): p. 325-34.

45. Wagner, B.J., et al., *Simvastatin reduces tumor cell adhesion to human peritoneal mesothelial cells by decreased expression of VCAM-1 and beta1 integrin.* Int J Oncol, 2011. **39**(6): p. 1593-600.
46. Rump, A., et al., *Binding of ovarian cancer antigen CA125/MUC16 to mesothelin mediates cell adhesion.* J Biol Chem, 2004. **279**(10): p. 9190-8.
47. Gubbels, J.A., et al., *Mesothelin-MUC16 binding is a high affinity, N-glycan dependent interaction that facilitates peritoneal metastasis of ovarian tumors.* Mol Cancer, 2006. **5**(1): p. 50.
48. Davidson, B., *Ovarian carcinoma and serous effusions. Changing views regarding tumor progression and review of current literature.* Anal Cell Pathol, 2001. **23**(3-4): p. 107-28.
49. Zhang, Y., et al., *Ovarian cancer-associated fibroblasts contribute to epithelial ovarian carcinoma metastasis by promoting angiogenesis, lymphangiogenesis and tumor cell invasion.* Cancer Lett, 2011. **303**(1): p. 47-55.
50. McLean, K., et al., *Human ovarian carcinoma-associated mesenchymal stem cells regulate cancer stem cells and tumorigenesis via altered BMP production.* J Clin Invest, 2011. **121**(8): p. 3206-19.
51. Huang, S., et al., *Blockade of nuclear factor-kappaB signaling inhibits angiogenesis and tumorigenicity of human ovarian cancer cells by suppressing expression of vascular endothelial growth factor and interleukin 8.* Cancer Res, 2000. **60**(19): p. 5334-9.
52. Kryczek, I., et al., *IL-6 production in ovarian carcinoma is associated with histiotype and biological characteristics of the tumour and influences local immunity.* Br J Cancer, 2000. **82**(3): p. 621-8.
53. Obata, N.H., et al., *Effects of interleukin-6 on in vitro cell attachment, migration and invasion of human ovarian carcinoma.* Anticancer Res, 1997. **17**(1A): p. 337-42.
54. Syed, V., et al., *Reproductive hormone-induced, STAT3-mediated interleukin 6 action in normal and malignant human ovarian surface epithelial cells.* J Natl Cancer Inst, 2002. **94**(8): p. 617-29.
55. Wang, Y., et al., *Autocrine production of interleukin-6 confers cisplatin and paclitaxel resistance in ovarian cancer cells.* Cancer Lett, 2010. **295**(1): p. 110-23.
56. Cohen, S., et al., *Platinum-resistance in ovarian cancer cells is mediated by IL-6 secretion via the increased expression of its target cIAP-2.* J Mol Med (Berl), 2013. **91**(3): p. 357-68.
57. Nilsson, M.B., R.R. Langley, and I.J. Fidler, *Interleukin-6, secreted by human ovarian carcinoma cells, is a potent proangiogenic cytokine.* Cancer Res, 2005. **65**(23): p. 10794-800.
58. Tempfer, C., et al., *Serum evaluation of interleukin 6 in ovarian cancer patients.* Gynecol Oncol, 1997. **66**(1): p. 27-30.
59. Scambia, G., et al., *Prognostic significance of interleukin 6 serum levels in patients with ovarian cancer.* Br J Cancer, 1995. **71**(2): p. 354-6.
60. Lane, D., et al., *Prognostic significance of IL-6 and IL-8 ascites levels in ovarian cancer patients.* BMC Cancer, 2011. **11**: p. 210.
61. Pradeep, S., et al., *Hematogenous metastasis of ovarian cancer: rethinking mode of spread.* Cancer Cell, 2014. **26**(1): p. 77-91.

62. Steeg, P.S., *Targeting metastasis.* Nat Rev Cancer, 2016. **16**(4): p. 201-18.
63. Massague, J. and A.C. Obenauf, *Metastatic colonization by circulating tumour cells.* Nature, 2016. **529**(7586): p. 298-306.
64. Greaves, M. and C.C. Maley, *Clonal evolution in cancer.* Nature, 2012. **481**(7381): p. 306-13.
65. Vanharanta, S. and J. Massague, *Origins of metastatic traits.* Cancer Cell, 2013. **24**(4): p. 410-21.
66. Zeimet, A.G., et al., *Ovarian cancer stem cells.* Neoplasma, 2012. **59**(6): p. 747-55.
67. Naora, H. and D.J. Montell, *Ovarian cancer metastasis: integrating insights from disparate model organisms.* Nat Rev Cancer, 2005. **5**(5): p. 355-66.
68. Ahmed, N., E.W. Thompson, and M.A. Quinn, *Epithelial-mesenchymal interconversions in normal ovarian surface epithelium and ovarian carcinomas: an exception to the norm.* J Cell Physiol, 2007. **213**(3): p. 581-8.
69. Hay, E.D., *An overview of epithelio-mesenchymal transformation.* Acta Anat (Basel), 1995. **154**(1): p. 8-20.
70. Thiery, J.P., et al., *Epithelial-mesenchymal transitions in development and disease.* Cell, 2009. **139**(5): p. 871-90.
71. Thiery, J.P. and J.P. Sleeman, *Complex networks orchestrate epithelial-mesenchymal transitions.* Nat Rev Mol Cell Biol, 2006. **7**(2): p. 131-42.
72. Kalluri, R. and R.A. Weinberg, *The basics of epithelial-mesenchymal transition.* J Clin Invest, 2009. **119**(6): p. 1420-8.
73. Huang, R.Y., P. Guilford, and J.P. Thiery, *Early events in cell adhesion and polarity during epithelial-mesenchymal transition.* J Cell Sci, 2012. **125**(Pt 19): p. 4417-22.
74. Peinado, H., D. Olmeda, and A. Cano, *Snail, Zeb and bHLH factors in tumour progression: an alliance against the epithelial phenotype?* Nat Rev Cancer, 2007. **7**(6): p. 415-28.
75. Vergara, D., et al., *Epithelial-mesenchymal transition in ovarian cancer.* Cancer Lett, 2010. **291**(1): p. 59-66.
76. Xu, J., S. Lamouille, and R. Derynck, *TGF-beta-induced epithelial to mesenchymal transition.* Cell Res, 2009. **19**(2): p. 156-72.
77. Batlle, E., et al., *The transcription factor snail is a repressor of E-cadherin gene expression in epithelial tumour cells.* Nat Cell Biol, 2000. **2**(2): p. 84-9.
78. Cano, A., et al., *The transcription factor snail controls epithelial-mesenchymal transitions by repressing E-cadherin expression.* Nat Cell Biol, 2000. **2**(2): p. 76-83.
79. Lin, T., et al., *Requirement of the histone demethylase LSD1 in Snai1-mediated transcriptional repression during epithelial-mesenchymal transition.* Oncogene, 2010. **29**(35): p. 4896-904.
80. Peinado, H., et al., *Snail mediates E-cadherin repression by the recruitment of the Sin3A/histone deacetylase 1 (HDAC1)/HDAC2 complex.* Mol Cell Biol, 2004. **24**(1): p. 306-19.
81. Tong, Z.T., et al., *EZH2 supports nasopharyngeal carcinoma cell aggressiveness by forming a co-repressor complex with HDAC1/HDAC2 and Snail to inhibit E-cadherin.* Oncogene, 2012. **31**(5): p. 583-94.

82. Herranz, N., et al., *Polycomb complex 2 is required for E-cadherin repression by the Snail1 transcription factor.* Mol Cell Biol, 2008. **28**(15): p. 4772-81.
83. Deng, J., et al., *The role of tumour-associated MUC1 in epithelial ovarian cancer metastasis and progression.* Cancer Metastasis Rev, 2013. **32**(3-4): p. 535-51.
84. Elloul, S., et al., *Snail, Slug, and Smad-interacting protein 1 as novel parameters of disease aggressiveness in metastatic ovarian and breast carcinoma.* Cancer, 2005. **103**(8): p. 1631-43.
85. Abdulkhalek, S., et al., *Transcriptional factor snail controls tumor neovascularization, growth and metastasis in mouse model of human ovarian carcinoma.* Clin Transl Med, 2014. **3**(1): p. 28.
86. Wang, Y.L., et al., *Snail promotes epithelial-mesenchymal transition and invasiveness in human ovarian cancer cells.* Int J Clin Exp Med, 2015. **8**(5): p. 7388-93.
87. Haslehurst, A.M., et al., *EMT transcription factors snail and slug directly contribute to cisplatin resistance in ovarian cancer.* BMC Cancer, 2012. **12**: p. 91.
88. Sanchez-Tillo, E., et al., *ZEB1 represses E-cadherin and induces an EMT by recruiting the SWI/SNF chromatin-remodeling protein BRG1.* Oncogene, 2010. **29**(24): p. 3490-500.
89. Elloul, S., et al., *Expression of E-cadherin transcriptional regulators in ovarian carcinoma.* Virchows Arch, 2006. **449**(5): p. 520-8.
90. Lamouille, S., et al., *Regulation of epithelial-mesenchymal and mesenchymal-epithelial transitions by microRNAs.* Curr Opin Cell Biol, 2013. **25**(2): p. 200-7.
91. Zhang, J., et al., *miR-30 inhibits TGF-beta1-induced epithelial-to-mesenchymal transition in hepatocyte by targeting Snail1.* Biochem Biophys Res Commun, 2012. **417**(3): p. 1100-5.
92. Gregory, P.A., et al., *The miR-200 family and miR-205 regulate epithelial to mesenchymal transition by targeting ZEB1 and SIP1.* Nat Cell Biol, 2008. **10**(5): p. 593-601.
93. Marchini, S., et al., *Association between miR-200c and the survival of patients with stage I epithelial ovarian cancer: a retrospective study of two independent tumour tissue collections.* Lancet Oncol, 2011. **12**(3): p. 273-85.
94. Nistico, P., M.J. Bissell, and D.C. Radisky, *Epithelial-mesenchymal transition: general principles and pathological relevance with special emphasis on the role of matrix metalloproteinases.* Cold Spring Harb Perspect Biol, 2012. **4**(2).
95. Tarin, D., E.W. Thompson, and D.F. Newgreen, *The fallacy of epithelial mesenchymal transition in neoplasia.* Cancer Res, 2005. **65**(14): p. 5996-6000; discussion 6000-1.
96. Zheng, X., et al., *Epithelial-to-mesenchymal transition is dispensable for metastasis but induces chemoresistance in pancreatic cancer.* Nature, 2015. **527**(7579): p. 525-30.
97. Fischer, K.R., et al., *Epithelial-to-mesenchymal transition is not required for lung metastasis but contributes to chemoresistance.* Nature, 2015. **527**(7579): p. 472-6.
98. Salamanca, C.M., et al., *Effects of epidermal growth factor/hydrocortisone on the growth and differentiation of human ovarian surface epithelium.* J Soc Gynecol Investig, 2004. **11**(4): p. 241-51.

99. Schipper, J.H., et al., *E-cadherin expression in squamous cell carcinomas of head and neck: inverse correlation with tumor dedifferentiation and lymph node metastasis.* Cancer Res, 1991. **51**(23 Pt 1): p. 6328-37.
100. Behrens, J., et al., *Cell adhesion in invasion and metastasis.* Semin Cell Biol, 1992. **3**(3): p. 169-78.
101. Morton, R.A., et al., *Reduction of E-cadherin levels and deletion of the alpha-catenin gene in human prostate cancer cells.* Cancer Res, 1993. **53**(15): p. 3585-90.
102. Davidowitz, R.A., et al., *Mesenchymal gene program-expressing ovarian cancer spheroids exhibit enhanced mesothelial clearance.* J Clin Invest, 2014. **124**(6): p. 2611-25.
103. Sundfeldt, K., *Cell-cell adhesion in the normal ovary and ovarian tumors of epithelial origin; an exception to the rule.* Mol Cell Endocrinol, 2003. **202**(1-2): p. 89-96.
104. Sundfeldt, K., et al., *E-cadherin expression in human epithelial ovarian cancer and normal ovary.* Int J Cancer, 1997. **74**(3): p. 275-80.
105. Latifi, A., et al., *Isolation and characterization of tumor cells from the ascites of ovarian cancer patients: molecular phenotype of chemoresistant ovarian tumors.* PLoS One, 2012. **7**(10): p. e46858.
106. Iwanicki, M.P., et al., *Ovarian cancer spheroids use myosin-generated force to clear the mesothelium.* Cancer Discov, 2011. **1**(2): p. 144-57.
107. Ahmed, N., et al., *Epithelial mesenchymal transition and cancer stem cell-like phenotypes facilitate chemoresistance in recurrent ovarian cancer.* Curr Cancer Drug Targets, 2010. **10**(3): p. 268-78.
108. Sutherland, R.M. and R.E. Durand, *Radiation response of multicell spheroids--an in vitro tumour model.* Curr Top Radiat Res Q, 1976. **11**(1): p. 87-139.
109. Sutherland, R.M., J.A. McCredie, and W.R. Inch, *Growth of multicell spheroids in tissue culture as a model of nodular carcinomas.* J Natl Cancer Inst, 1971. **46**(1): p. 113-20.
110. Desoize, B. and J. Jardillier, *Multicellular resistance: a paradigm for clinical resistance?* Crit Rev Oncol Hematol, 2000. **36**(2-3): p. 193-207.
111. Kantak, S.S. and R.H. Kramer, *E-cadherin regulates anchorage-independent growth and survival in oral squamous cell carcinoma cells.* J Biol Chem, 1998. **273**(27): p. 16953-61.
112. Zietarska, M., et al., *Molecular description of a 3D in vitro model for the study of epithelial ovarian cancer (EOC).* Mol Carcinog, 2007. **46**(10): p. 872-85.
113. Puiffe, M.L., et al., *Characterization of ovarian cancer ascites on cell invasion, proliferation, spheroid formation, and gene expression in an in vitro model of epithelial ovarian cancer.* Neoplasia, 2007. **9**(10): p. 820-9.
114. Zhang, S., et al., *Identification and characterization of ovarian cancer-initiating cells from primary human tumors.* Cancer Res, 2008. **68**(11): p. 4311-20.
115. Shield, K., et al., *Multicellular spheroids in ovarian cancer metastases: Biology and pathology.* Gynecol Oncol, 2009. **113**(1): p. 143-8.
116. Wintzell, M., et al., *Protein markers of cancer-associated fibroblasts and tumor-initiating cells reveal subpopulations in freshly isolated ovarian cancer ascites.* BMC Cancer, 2012. **12**: p. 359.
117. Casey, R.C., et al., *Beta 1-integrins regulate the formation and adhesion of ovarian carcinoma multicellular spheroids.* Am J Pathol, 2001. **159**(6): p. 2071-80.

118. Achilli, T.M., J. Meyer, and J.R. Morgan, *Advances in the formation, use and understanding of multi-cellular spheroids.* Expert Opin Biol Ther, 2012. **12**(10): p. 1347-60.
119. LaBarbera, D.V., B.G. Reid, and B.H. Yoo, *The multicellular tumor spheroid model for high-throughput cancer drug discovery.* Expert Opin Drug Discov, 2012. **7**(9): p. 819-30.
120. Provencher, D.M., et al., *Characterization of four novel epithelial ovarian cancer cell lines.* In Vitro Cell Dev Biol Anim, 2000. **36**(6): p. 357-61.
121. Domcke, S., et al., *Evaluating cell lines as tumour models by comparison of genomic profiles.* Nat Commun, 2013. **4**: p. 2126.
122. Kobel, M., et al., *Biomarker expression in pelvic high-grade serous carcinoma: comparison of ovarian and omental sites.* Int J Gynecol Pathol, 2011. **30**(4): p. 366-71.
123. Cody, N.A., et al., *Transfer of chromosome 3 fragments suppresses tumorigenicity of an ovarian cancer cell line monoallelic for chromosome 3p.* Oncogene, 2007. **26**(4): p. 618-32.
124. Huang, R.Y., et al., *An EMT spectrum defines an anoikis-resistant and spheroidogenic intermediate mesenchymal state that is sensitive to e-cadherin restoration by a src-kinase inhibitor, saracatinib (AZD0530).* Cell Death Dis, 2013. **4**: p. e915.
125. Lamouille, S., J. Xu, and R. Derynck, *Molecular mechanisms of epithelial-mesenchymal transition.* Nat Rev Mol Cell Biol, 2014. **15**(3): p. 178-96.
126. Wu, Y. and B.P. Zhou, *Snail: More than EMT.* Cell Adh Migr, 2010. **4**(2): p. 199-203.
127. Brabletz, S. and T. Brabletz, *The ZEB/miR-200 feedback loop--a motor of cellular plasticity in development and cancer?* EMBO Rep, 2010. **11**(9): p. 670-7.
128. Sokol, E.S., et al., *Growth of human breast tissues from patient cells in 3D hydrogel scaffolds.* Breast Cancer Res, 2016. **18**(1): p. 19.
129. Moss, N.M., et al., *Ovarian cancer cell detachment and multicellular aggregate formation are regulated by membrane type 1 matrix metalloproteinase: a potential role in I.p. metastatic dissemination.* Cancer Res, 2009. **69**(17): p. 7121-9.
130. Pettee, K.M., et al., *An mDia2/ROCK signaling axis regulates invasive egress from epithelial ovarian cancer spheroids.* PLoS One, 2014. **9**(2): p. e90371.
131. McGrail, D.J., Q.M. Kieu, and M.R. Dawson, *The malignancy of metastatic ovarian cancer cells is increased on soft matrices through a mechanosensitive Rho-ROCK pathway.* J Cell Sci, 2014. **127**(Pt 12): p. 2621-6.
132. Jemal, A., et al., *Cancer statistics, 2005.* CA Cancer J Clin, 2005. **55**(1): p. 10-30.
133. Siegel, R.L., K.D. Miller, and A. Jemal, *Cancer statistics, 2015.* CA Cancer J Clin, 2015. **65**(1): p. 5-29.
134. Mackay, H.J., et al., *A phase II trial of the Src kinase inhibitor saracatinib (AZD0530) in patients with metastatic or locally advanced gastric or gastro esophageal junction (GEJ) adenocarcinoma: a trial of the PMH phase II consortium.* Invest New Drugs, 2012. **30**(3): p. 1158-63.
135. Cattau, E.L., Jr., et al., *The accuracy of the physical examination in the diagnosis of suspected ascites.* Jama, 1982. **247**(8): p. 1164-6.
136. Sheid, B., *Angiogenic effects of macrophages isolated from ascitic fluid aspirated from women with advanced ovarian cancer.* Cancer Lett, 1992. **62**(2): p. 153-8.

137. Aceto, N., et al., *Circulating tumor cell clusters are oligoclonal precursors of breast cancer metastasis.* Cell, 2014. **158**(5): p. 1110-22.
138. Labelle, M. and R.O. Hynes, *The initial hours of metastasis: the importance of cooperative host-tumor cell interactions during hematogenous dissemination.* Cancer Discov, 2012. **2**(12): p. 1091-9.
139. Chambers, A.F., et al., *Molecular biology of breast cancer metastasis. Clinical implications of experimental studies on metastatic inefficiency.* Breast Cancer Res, 2000. **2**(6): p. 400-7.
140. Browne, G., A.E. Sayan, and E. Tulchinsky, *ZEB proteins link cell motility with cell cycle control and cell survival in cancer.* Cell Cycle, 2010. **9**(5): p. 886-91.
141. Lu, Z.Y., et al., *SNAI1 overexpression induces stemness and promotes ovarian cancer cell invasion and metastasis.* Oncol Rep, 2012. **27**(5): p. 1587-91.
142. Muqbil, I., et al., *Snail nuclear transport: the gateways regulating epithelial-to-mesenchymal transition?* Semin Cancer Biol, 2014. **27**: p. 39-45.
143. Liu, Y., et al., *Different thresholds of ZEB1 are required for Ras-mediated tumour initiation and metastasis.* Nat Commun, 2014. **5**: p. 5660.
144. Eger, A., et al., *DeltaEF1 is a transcriptional repressor of E-cadherin and regulates epithelial plasticity in breast cancer cells.* Oncogene, 2005. **24**(14): p. 2375-85.
145. Lehmann, W., et al., *ZEB1 turns into a transcriptional activator by interacting with YAP1 in aggressive cancer types.* Nat Commun, 2016. **7**: p. 10498.
146. Yagi, H., et al., *GEP oncogene promotes cell proliferation through YAP activation in ovarian cancer.* Oncogene, 2016.
147. Yu, F.X., B. Zhao, and K.L. Guan, *Hippo Pathway in Organ Size Control, Tissue Homeostasis, and Cancer.* Cell, 2015. **163**(4): p. 811-28.
148. Dominguez, D., et al., *Phosphorylation regulates the subcellular location and activity of the snail transcriptional repressor.* Mol Cell Biol, 2003. **23**(14): p. 5078-89.
149. Zhou, B.P., et al., *Dual regulation of Snail by GSK-3beta-mediated phosphorylation in control of epithelial-mesenchymal transition.* Nat Cell Biol, 2004. **6**(10): p. 931-40.
150. Yang, Z., et al., *Pak1 phosphorylation of snail, a master regulator of epithelial-to-mesenchyme transition, modulates snail's subcellular localization and functions.* Cancer Res, 2005. **65**(8): p. 3179-84.
151. Du, C., et al., *Protein kinase D1 suppresses epithelial-to-mesenchymal transition through phosphorylation of snail.* Cancer Res, 2010. **70**(20): p. 7810-9.
152. Lin, C.Y., et al., *Matrix metalloproteinase-9 cooperates with transcription factor Snail to induce epithelial-mesenchymal transition.* Cancer Sci, 2011. **102**(4): p. 815-27.
153. Yang, Z., et al., *Co-targeting EGFR and Autophagy Impairs Ovarian Cancer Cell Survival during Detachment from the ECM.* Curr Cancer Drug Targets, 2015. **15**(3): p. 215-26.
154. Bracken, C.P., et al., *A double-negative feedback loop between ZEB1-SIP1 and the microRNA-200 family regulates epithelial-mesenchymal transition.* Cancer Res, 2008. **68**(19): p. 7846-54.
155. Friedl, P., *Prespecification and plasticity: shifting mechanisms of cell migration.* Curr Opin Cell Biol, 2004. **16**(1): p. 14-23.

156. Sanz-Moreno, V. and C.J. Marshall, *The plasticity of cytoskeletal dynamics underlying neoplastic cell migration.* Curr Opin Cell Biol, 2010. **22**(5): p. 690-6.
157. Wolf, K., et al., *Compensation mechanism in tumor cell migration: mesenchymal-amoeboid transition after blocking of pericellular proteolysis.* J Cell Biol, 2003. **160**(2): p. 267-77.
158. Beaufort, C.M., et al., *Ovarian cancer cell line panel (OCCP): clinical importance of in vitro morphological subtypes.* PLoS One, 2014. **9**(9): p. e103988.

APPENDIX

A1: LICENSE: REUSE OF FIGURE

Figure 1 was reused from Nature Reviews Molecular Cell Biology, from the publication titled: Ovary and fimbrial stem cells: biology, niche and cancer origins. A license was obtained through Copyrights Clearance Center's RightsLink service that Nature Publishing Group partners with. Below are the license details:

Licensee: Sara Al-Habyan

License Date: Mar 10, 2016

License Number: 3825521495779

Type Of Use: reuse in dissertation / thesis

FIGURE A2: HEAT MAP OF RT-QPCR RESULTS

The heat map below provides an overview analysis of average expression fold changes across all genes included in the array. Comments are defined as follows by QIAGEN data sampler tool.

A: "This gene's average threshold cycle is relatively high in one sample, and relatively low in the other sample.. suggesting that the actual fold change value is at least and large as the calculated and reported fold-change result"

B: " This gene's average threshold cycle is relatively high.. in both samples"

C: " This gene's average threshold cycle is either not determined or greater than defined cut-off in both samples meaning that its expression was undetected, making this fold change result un-interpretable."

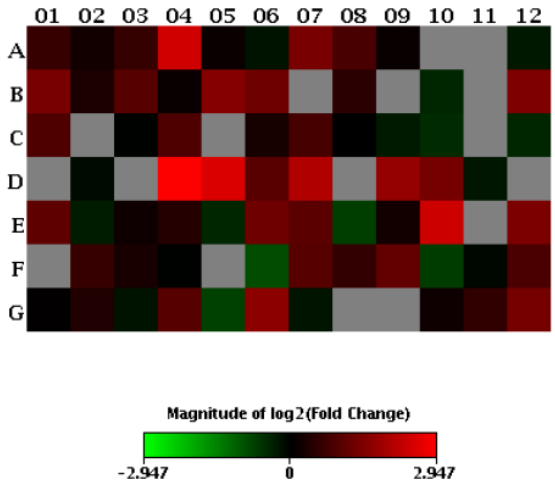

Layout	01	02	03	04	05	06	07	08	09	10	11	12
A	AHNAK 1.54 A	AKT1 1.16	BMP1 1.52 B	BMP2 5.29 A	BMP7 1.08 B	CALD1 -1.15	CAMK2N1 2.62 B	CAV2 1.78	CDH1 1.06 A	CDH2 3.38 C	COL1A2 3.38 C	COL3A1 -1.22 A
B	COL5A2 2.62 B	CTNNB1 1.24 B	DSC2 2.00 B	DSP 1.07	EGFR 2.93	ERBB3 2.40 B	ESR1 3.38 C	F11R 1.40	FGFBP1 3.38 C	FN1 -1.36	FOXC2 3.38 C	FZD7 2.74 B
C	GNG11 1.88 B	GSC 3.38 C	GSK3B -1.01 A	IGFBP4 1.86 A	IL1RN 3.38 C	ILK 1.19 A	ITGA5 1.77 A	ITGAV -1.00 A	ITGB1 -1.22	JAG1 -1.39	KRT14 3.38 C	KRT19 -1.36
D	KRT7 3.38 C	MAP1B -1.09 A	MMP2 3.38 C	MMP3 7.71 B	MMP9 5.80	MSN 2.03	MST1R 4.14	NODAL 3.38 C	NOTCH1 3.31 B	NUDT13 2.51 B	OCLN -1.18	PDGFRB 3.38 C
E	PLEK2 2.11 B	DESI1 -1.25 A	PTK2 1.12 A	PTP4A1 1.33	RAC1 -1.36	RGS2 2.42 A	SERPINE1 2.05	GEMIN2 -1.64 A	SMAD2 1.16 A	SNAI1 5.17	SNAI2 3.38 C	SNAI3 2.69
F	SOX10 3.38 C	SPARC 1.55 B	SPP1 1.21	STAT3 -1.02	STEAP1 3.38 C	TCF3 -1.83 A	TCF4 1.98 B	TFPI2 1.49	TGFB1 2.19	TGFB2 -1.61 A	TGFB3 -1.05 B	TIMP1 1.82
G	TMEFF1 1.02 B	TMEM132A 1.29 B	TSPAN13 -1.15 A	TWIST1 2.00 B	VCAN -1.67 A	VIM 3.12 B	VPS13A -1.18 B	WNT11 3.38 C	WNT5A 3.38 C	WNT5B 1.11 B	ZEB1 1.46 B	ZEB2 2.54 B